NASA Contractor Report 189738
ICASE Report No. 92–65

ICASE

THE STABILITY OF A TRAILING-LINE VORTEX IN COMPRESSIBLE FLOW

Jillian A. K. Stott
Peter W. Duck

NASA Contract Nos. NAS1–18605 and NAS1–19480
December 1992

Institute for Computer Applications in Science and Engineering
NASA Langley Research Center
Hampton, Virginia 23681–0001

Operated by the Universities Space Research Association

National Aeronautics and
Space Administration

Langley Research Center
Hampton, Virginia 23665-5225

THE STABILITY OF A TRAILING-LINE VORTEX IN COMPRESSIBLE FLOW

Jillian A. K. Stott and Peter W. Duck[1]

Department of Mathematics
University of Manchester
Manchester, M13 9PL
UNITED KINGDOM

ABSTRACT

We consider the inviscid stability of the Batchelor (1964) vortex in a compressible flow. The problem is tackled numerically and also asymptotically, in the limit of large (azimuthal and streamwise) wavenumbers, together with large Mach numbers. The nature of the solution passes through different regimes as the Mach number increases, relative to the wavenumbers. At very high wavenumbers and Mach numbers, the mode which is present in the incompressible case ceases to be unstable, whilst a new "centre mode" forms, whose stability characteristics are determined primarily by conditions close to the vortex axis. We find that generally the flow becomes less unstable as the Mach number increases, and that the regime of instability appears generally confined to disturbances in a direction counter to the direction of the rotation of the swirl of the vortex.

Throughout the paper comparison is made between our numerical results and results obtained from the various asymptotic theories.

[1]This research was supported by the National Aeronautics and Space Administration under NASA Contract Nos. NAS1-18605 and NAS1-19480 while the second author was in residence at the Institute for Computer Applications in Science and Engineering (ICASE), NASA Langley Research Center, Hampton, VA 23681.

1. Introduction

In recent years there has been a good deal of interest in the stability of incompressible swirling vortex–type flows. Two important applications to this area of research are the breakdown of trailing–line vortices behind aircraft and to tornadoes; this class of flow may also be applicable to flows inside turbines and compressors, to which the present work would be particularly relevant.

The earliest works in the area of the stability of swirling vortex flows include those of Lessen & Paillet (1974) and Lessen, Singh & Paillet (1974). In the former paper the stability of the Batchelor (1964) vortex was considered, at finite Reynolds numbers up to 150. In the second paper, the inviscid stability of this vortex was studied and revealed an increase in growth rate at increasingly large wavenumbers (with disturbances being most dangerous counter to the direction of the swirl).

Duck & Foster (1980) showed that for a given wavenumber a multiplicity of modes exists. Leibovich & Stewartson (1983) and Duck (1986) considered the limit of large wavenumber for this problem, and showed that a finite (maximum) growth rate was attained. The aforementioned studies suggested an upper and lower neutral value of axial wavenumber. The upper neutral point for large azimuthal wavenumber was treated by Stewartson & Capell (1985), who showed that the "ring mode" structure of the unstable modes persisted near the upper neutral points. Stewartson & Brown (1985) considered these upper neutral points for order one azimuthal wavenumbers, and found that in this case the modes were of centre mode type, similar to those found in a related study on swirling Poiseuille flow (Stewartson & Brown 1984). The behaviour of the unstable modes, close to the lower neutral point, at large azimuthal wavenumber, was investigated by Stewartson & Leibovich (1987), and determined that in this case the instability disturbances were centred near the axis of the vortex.

More recently, viscous results have been presented at finite (but large) Reynolds numbers by Khorrami *et al.* (1989) and Khorrami (1991). In this latter paper, it was shown that additional unstable modes exist, in which viscosity plays a destabilising role. These modes were analysed by Duck & Khorrami (1991). The inviscid analysis is also

applicable to other vortex profiles, including that of Long (1961), as studied by Foster & Duck (1982) and Foster & Smith (1989).

Little attention has been paid to the stability of compressible vortex flows of this type. On the other hand the area of compressible jet flow has been investigated for some years now, the work of Michalke (1971, 1984) being relevant here, although restricted to non–swirling flows. Compressible swirling jet flows have also received some attention, the work of Coleman (1989) should be mentioned, who studied the superposition of a Rankine vortex on a top–hat jet velocity field. More recently, Khorrami (1991) studied a compressible swirling axisymmetric jet, by assuming the incompressible flow of Görtler (1954) and Loitsyanskii (1953) was applicable in the compressible regime.

In this paper, we take cylindrical polar coordinates, (lr, θ, lx), with the x axis lying along the axis of the vortex (which is taken to be axisymmetric), and l is some streamwise scale. We also take the flow far from the vortex centre to be directed along the x–direction. The velocity field is written as $U_s^*\mathbf{u} = U_s^*(u, v, w)$, the fluid density is $\rho_\infty^*\rho$, temperature T_∞^*T, first and second coefficients of viscosity $\mu_\infty^*\mu$, $\mu_\infty^*\lambda$ respectively, and pressure $\rho_\infty^* U_s^{*2} p$. Here superscript asterisk and subscript ∞ denote dimensional and freestream variables, respectively, and also U_s^* is a velocity scale, defined below in (2.6), whilst U_∞^* is the freestream velocity. We define the flow Reynolds number

$$Re = \frac{\rho_\infty^* U_s^* l}{\mu_\infty^*} \tag{1.1}$$

and we have a flow Mach number given by

$$M = \frac{U_s^*}{(\gamma R^* T_\infty^*)^{\frac{1}{2}}}, \tag{1.2}$$

where γ is the ratio of specific heats and R^* the gas constant. We also define the Prandtl number to be

$$\sigma = \frac{\mu^* c_p}{\kappa^*}, \tag{1.3}$$

where κ^* is the thermal conductivity of the fluid.

The non–dimensional equations of continuity, momentum and energy may then be written

$$\frac{\partial \rho}{\partial t} + \nabla.(\rho \mathbf{u}) = 0, \tag{1.4}$$

$$\rho \frac{D\mathbf{u}}{Dt} = -\nabla p - \frac{1}{Re}\nabla \wedge [\mu(\nabla \wedge \mathbf{u})] + \frac{1}{Re}\nabla.[(\lambda + 2\mu)\nabla.\mathbf{u}], \tag{1.5}$$

$$\rho \frac{Dh}{Dt} = \frac{Dp}{Dt} + \Phi + \frac{1}{\sigma Re}\nabla.(\mu \nabla T), \tag{1.6}$$

where h is the enthalpy of the fluid, and Φ is the viscous dissipation. We also assume a perfect gas, in which case we have

$$p = \frac{\rho T}{\gamma M^2}. \tag{1.7}$$

In the following sections we consider first the basic flow (section 2), which is shown to be a proper solution of the above equations of continuity, momentum and energy. In section 3 we consider the inviscid linear stability equations. In section 4 we present a number of numerical results, guided by which, in section 5 we develop asymptotic results for large wavenumbers; throughout this section we emphasise a comparison between our numerical and asymptotic results. In section 6 a new class of mode, which is found to develop at sufficiently large Mach number is considered. In section 7 we present a number of conclusions arising from this work.

2. The basic flow

Let us consider the solution corresponding to Batchelors' (1964) similarity solution for a swirling wake flow, equivalent to a far downstream limit ($x \gg 1$) of the governing equations. We thus suppose that the solution comprises of a uniform (freestream) flow plus a relatively small perturbation, i.e.

$$u = \frac{U^*_\infty}{U^*_s} + \tilde{u}, \tag{2.1a}$$

$$v = \tilde{v}, \tag{2.1b}$$

$$w = \tilde{w}, \tag{2.1c}$$

$$p = \frac{{U^*_\infty}^2}{{U^*_s}^2} + \tilde{p}, \tag{2.1d}$$

$$T = 1 + \widetilde{T}, \tag{2.1e}$$

$$\rho = 1 + \tilde{\rho}. \tag{2.1f}$$

The solution develops in much the same way as the incompressible case of Batchelor (1964) and it is found to leading order that

$$\tilde{u} = \frac{1}{U^*_s}\left(-\frac{C_0^2 U^*_\infty \log(xRe_\infty)}{8x{\nu^*_\infty}^2 Re_\infty}Q_1(\eta) + \frac{C_0^2 U^*_\infty}{8x{\nu^*_\infty}^2 Re_\infty}Q_2(\eta) - \frac{L{U^*_\infty}^2 e^{-\eta}}{8x{\nu^*_\infty}^2 Re_\infty}\right), \tag{2.2}$$

$$\tilde{v} = 0 \tag{2.3}$$

$$\tilde{w} = \frac{C_0 Re_\infty^{\frac{1}{2}}}{2(x\eta)^{\frac{1}{2}}U^*_s}(1 - e^{-\eta}), \tag{2.4}$$

where

$$\eta = \frac{\hat{r}^2 Re_\infty}{4x}, \tag{2.5}$$

$$U^*_s = \frac{C_0^2 U^*_\infty}{8x{\nu^*_\infty}^2 Re_\infty}\log(xRe_\infty) + \frac{L{U^*_\infty}^2}{8x{\nu^*_\infty}^2 Re_\infty}, \tag{2.6}$$

and

$$Q_1(\eta) = e^{-\eta}, \tag{2.7a}$$

$$Q_2(\eta) = e^{-\eta}[\log\eta + ei(\eta) - 0.867] + 2ei(\eta). \tag{2.7b}$$

C_0 and L are constants and Re_∞ is the freestream Reynolds number defined by

$$Re_\infty = \frac{\rho^*_\infty U^*_\infty l}{\mu^*_\infty}. \tag{2.8}$$

We also find that

$$\tilde{p} = \frac{C_0^2 {U^*_\infty}^2}{8x{\nu^*_\infty}^2 {U^*_s}^2 Re_\infty}\Big[\frac{(1-e^{-\eta})^2}{\eta} + 2ei(\eta) - 2ei(2\eta)\Big], \tag{2.9}$$

whilst the temperature perturbation is given by

$$\begin{aligned}\widetilde{T} = e^{-\frac{\sigma\xi^2}{4}}\Bigg(&\frac{A}{2}ei(\frac{1}{4}\sigma\xi^2) + B + \frac{(\gamma-1)M_\infty^2 C_0^2}{8x{\nu^*_\infty}^2 Re_\infty}\Big[ei\Big((\frac{1}{4}\sigma - \frac{1}{4})\xi^2\Big)\\
&+\int\Big(-8\sigma\frac{e^{\frac{\sigma\xi^2}{4}}}{\xi^2} + 16\sigma\frac{e^{\frac{1}{4}(\sigma-1)\xi^2}}{\xi^2}\\
&+\frac{8\sigma\pi^{\frac{1}{2}}}{\xi}e^{\frac{\sigma\xi^2}{4}}erf(\xi/2) - 8\frac{e^{(\frac{\sigma}{4}-\frac{1}{2})\xi^2}}{\xi^2} - 4\frac{\sigma 2\pi^{\frac{1}{2}}}{x}e^{\frac{\sigma\xi^2}{4}}erf(\xi/2^{\frac{1}{2}})\Big)d\xi\\
&+\int e^{\frac{\sigma\xi^2}{4}}\int\frac{1}{\xi}\Big(-2\sigma\big(-2e^{\frac{\xi^2}{4}} + 2 - \xi^2 e^{\frac{\xi^2}{4}}ei(\xi^2/4)\\
&\qquad +\xi^2 e^{\frac{\xi^2}{4}}ei(\xi^2/2)\big) + \frac{e^{-\frac{\xi^2}{4}}}{\xi}\Big)d\xi d\xi\Big]\Bigg),\end{aligned} \tag{2.10}$$

where A and B are constants, $\xi = 2\eta^{\frac{1}{2}}$, $ei(z)$ and $erf(z)$ are the exponential integral and the error function, respectively, defined in the normal manner, and M_∞ is the freestream Mach number defined by

$$M_\infty = \frac{U^*_\infty}{(\gamma R^* T^*_\infty)^{\frac{1}{2}}} = \frac{U^*_\infty}{U^*_s}M. \tag{2.11}$$

Note that we expect $M_\infty \gg M$. We also find it useful for the remainder of the paper to define the lengthscale

$$r = \eta^{\frac{1}{2}} = \frac{\hat{r}}{r_s}, \tag{2.12}$$

where $r_s = (4x/Re_\infty)^{\frac{1}{2}}$ is the characteristic radial lengthscale.

In the following section we consider the inviscid stability equations.

3. The stability equations

We take the general basic state to be $u = U(r), v = 0, w = W(r), T = T_0(r), p = p_0(r), \rho = \rho_0(r)$ and consider small amplitude perturbations to this flow; we write

$$u = U(r) + \delta F(r)E + \mathrm{O}(\delta^2), \tag{3.1a}$$

$$v = i\delta G(r)E + \mathrm{O}(\delta^2), \tag{3.1b}$$

$$w = W(r) + \delta H(r)E + \mathrm{O}(\delta^2), \tag{3.1c}$$

$$p = p_0(r) + \delta\gamma M^2 P(r)E + \mathrm{O}(\delta^2), \tag{3.1d}$$

$$T = T_0(r) + \delta\tau(r)E + \mathrm{O}(\delta^2), \tag{3.1e}$$

$$\rho = \rho_0(r) + \delta\Gamma(r)E + \mathrm{O}(\delta^2), \tag{3.1f}$$

where, $\delta \ll 1$, and

$$E = \exp[i(\alpha x/r_s + n\theta - \alpha ct/r_s)]. \tag{3.1g}$$

The governing stability equations, neglecting the effects of viscosity are then

$$\Gamma\varphi + \rho_0\Big(\alpha F + G' + \frac{G}{r} + \frac{nH}{r}\Big) + G\rho_0' = 0, \tag{3.2}$$

$$\rho_0\varphi F + \rho_0 U'G = -\alpha P, \tag{3.3}$$

$$\rho_0\varphi G + \rho_0\frac{2WH}{r} + \frac{\Gamma W^2}{r} = P', \tag{3.4}$$

$$\rho_0\varphi H + \rho_0\Big(W' + \frac{W}{r}\Big)G = -\frac{nP}{r}, \tag{3.5}$$

$$\rho_0\varphi\tau + \rho_0 GT_0'(r) - \left(\frac{\gamma-1}{\gamma}\right)(\gamma\varphi M^2 P + Gp_0') = 0, \tag{3.6}$$

$$\gamma M^2 P = \Gamma T_0 + \tau\rho_0, \tag{3.7}$$

where we have written

$$\varphi = \alpha(U - c) + \frac{nW}{r}, \tag{3.8}$$

and primes denote differentiation with respect to r. Note that (3.1), (3.2)—(3.7) all implicitly assume that the axial scale for the perturbation quantities is considerably shorter than any developmental lengthscale for the basic flow, as is the case if $r_s \ll 1$.

Equations (3.2)–(3.7) may be combined to yield the following two, first order equations

$$\frac{dG}{dr} = \Big[\frac{n(rW)' + \alpha r^2 U'}{r^2\varphi} - \frac{p_0'}{\gamma p_0} - \frac{1}{r}\Big]G + \frac{1}{\rho_0}\Big[\frac{(\alpha^2 r^2 + n^2)}{r^2\varphi} - \frac{\varphi M^2}{T_0}\Big]P, \tag{3.9}$$

$$\frac{dP}{dr} = \rho_0\Big[\varphi - \frac{(W^2r^2)'}{r^3\varphi} - \frac{W^2}{r\varphi}\Big(-\frac{T_0'}{T_0} + \Big(\frac{\gamma-1}{\gamma}\Big)\frac{p_0'}{\rho_0 T_0}\Big)\Big]G$$
$$-\Big[\frac{2nW}{r^2\varphi} - \frac{W^2M^2}{rT_0}\Big]P. \tag{3.10}$$

These equations are somewhat similar to those considered by Michalke (1971), in the context of jet flows, if the swirl velocity is neglected.

Let us now consider the specific basic flow of the trailing line vortex, as discussed in the previous section. Equations (2.1), (2.3)—(2.5) may be substituted into (3.9), (3.10), and then if we assume $|\delta| \ll |\frac{1}{x}\log x|$, and using the fact that a simple transformation and inversion of the axial velocity only affects the frequency of the stability analysis, and does not change the amplification factor c_i (where $c = c_r + ic_i$) and noting that $\tilde{p}$, $\tilde{\rho}$ and $\tilde{T}$ are an order of $\mathrm{O}(\log x)$ smaller than $\tilde{u}$, $\tilde{v}$ and $\tilde{w}$, then (3.9), (3.10) reduce to

$$\frac{dG}{dr} = \Big[\frac{n(rW)' + \alpha r^2 U'}{r^2\varphi} - \frac{1}{r}\Big]G + \Big[\frac{\alpha^2 r^2 + n^2}{r^2\varphi} - \varphi M^2\Big]P, \tag{3.11}$$

$$\frac{dP}{dr} = \Big[\varphi - \frac{(W^2r^2)'}{r^3\varphi}\Big]G - \Big[\frac{2nW}{r^2\varphi} - \frac{W^2M^2}{r}\Big]P. \tag{3.12}$$

The boundary conditions to be applied are then

$$P(0) = 0,\ n \neq 0; \quad P'(0),\ n = 0,$$

$$G(0) = 0,\ |n| \neq 1; \quad G'(0),\ |n| = 1,$$

$$\text{and } G(r),\ P(r) \text{ bounded as } r \to \infty, \tag{3.13}$$

and the basic flow may be taken to be

$$U = e^{-r^2}, \tag{3.14}$$

$$W = \frac{q}{r}(1 - e^{-r^2}), \tag{3.15}$$

where q is an order one (swirl) parameter, and we have effectively scaled velocities with respect to U_s^*.

Equations (3.11), (3.12) may be combined to eliminate G, yielding the following second–order equation for P.

$$\begin{aligned} P_{rr} + P_r\Bigg\{ & \frac{2nW}{r^2\varphi} - \frac{W^2M^2}{r} + \frac{1}{r} - \left[\varphi - \frac{(W^2r^2)'}{r^3\varphi}\right]' \Big/ \left[\varphi - \frac{(W^2r^2)'}{r^3\varphi}\right] \\ & - \frac{[\alpha r^2U' + n(rW)']}{r^2\varphi}\Bigg\} + P\Bigg\{\left[\frac{2nW}{r^2\varphi} - \frac{W^2M^2}{r}\right]' \\ & - \left[\frac{2nW}{r^2\varphi} - \frac{W^2M^2}{r}\right]\left[\varphi - \frac{(W^2r^2)'}{r^3\varphi}\right]' \Big/ \left[\varphi - \frac{(W^2r^2)'}{r^3\varphi}\right] \\ & + \left(\frac{1}{r} - \frac{[\alpha r^2U' + n(rW)']}{r^2\varphi}\right)\left[\frac{2nW}{r^2\varphi} - \frac{W^2M^2}{r}\right] \\ & - \left[\frac{\alpha^2r^2 + n^2}{r^2\varphi} - \varphi M^2\right]\left[\varphi - \frac{(W^2r^2)'}{r^3\varphi}\right]\Bigg\} = 0. \end{aligned} \tag{3.16}$$

Setting $M = 0$ clearly reduces (3.11), (3.12) and (3.16) to the incompressible problem, as considered by Lessen *et al.* (1974), Duck & Foster (1980), Leibovich & Stewartson (1983) and Duck (1986). It is also possible to be rather more precise regarding the behaviour of the solution as $r \to \infty$; this takes the form

$$\frac{dG}{dr} \pm \alpha(1 - c^2M^2)^{\frac{1}{2}}G = 0, \tag{3.17}$$

$$\frac{dP}{dr} \pm \alpha(1 - c^2M^2)^{\frac{1}{2}}P = 0, \tag{3.18}$$

where positive signs are taken for $\Re\{(1 - c^2M^2)^{\frac{1}{2}}\} > 0$, and vice versa, to ensure boundedness as $r \to \infty$.

The "order one" problem requires a fully numerical solution, which we consider in the following section, prior to considering various asymptotic limits of this system of equations, which permit a certain amount of analytical progress.

4. Numerical results

The system was treated numerically using four different techniques. The first was based on the method of Duck & Foster (1980), in which the system was approximated by second–order central differences, with conditions (3.17) and (3.18) imposed at a finite radial value $r = r_{max}$, taken sufficiently large not to substantially affect the result. The determinant of the system was then forced to zero by adjusting the complex wavespeed c (using Newton iteration).

The second method was based on a fourth–order Runge–Kutta scheme, conditions (3.17) and (3.18) were approximated by imposing boundary conditions at a finite radial value $r = r_{max}$, where this value was again taken sufficiently large to not substantially affect the numerical results. The computations were performed by shooting the solution towards $r = 0$ and were not necessarily confined to the real r–axis. The value of c was adjusted (again using Newton iteration), to ensure the correct behaviour of the solution as $r \to 0$.

The third method used was based on the first, but was a global finite difference method. Using the aforementioned finite–difference scheme, then by defining two additional quantities $\widehat{G} = cG$, $\widehat{P} = cP$ at each grid point, it is possible to write the resulting scheme in the form

$$(\mathbf{A} - c\mathbf{B})\mathbf{x} = 0, \tag{4.1}$$

where

$$\mathbf{x} = \left[\{G\},\ \{P\},\ \{\widehat{G}\},\ \{\widehat{P}\}\right]^T. \tag{4.2}$$

This scheme has the obvious advantage of generating $4N$ eigenvalues (where N is the number of grid points), simultaneously. The principle disadvantages are (i) it is not possible to use (3.17) or (3.18) because of the non–linearity of c, and consequently Dirichlet boundary conditions were applied instead at the outer edge of the computational domain; and (ii) the scheme requires rapidly increasing computational resources (both in storage and time) as N increases.

The fourth scheme implemented was a Chebyshev spectral collocation scheme, based on that of Khorrami, Ash & Malik (1989). This was a global method, which generally gave very accurate eigenvalues, but also yielded a large number of spurious eigenvalues, a feature found in many spectral schemes. The first (finite–difference) scheme was quick and robust, but because of its "local" nature, mode jumping was often experienced, due to the frequent close proximity of neighbouring modes, as discussed later in the paper. The second (Runge–Kutta) scheme was also quite fast, and had the advantage of being able to compute neutral and near–neutral modes (and even stable modes) by contour indentation, but again because it involved local searching was prone to mode jumping. The third scheme, namely the global finite–difference scheme, which proved to be very robust, produced few, if any spurious (i.e. non–physical) modes, and generated many eigenvalues simultaneously because of its global nature. Consequently our results were generally computed using the first scheme (if only a limited number of modes were required) or the third scheme if it was required to compute many modes.

We now present a few numerical results to give some indication of the effects of variation of certain of the important parameters. Here, and indeed in all our calculations we chose $\gamma = 1.4$, $q = 0.8$. Further, we generally found that $r_{max} = 5$ was sufficient with $\Delta r \approx 0.03$.

Figures 1 a, b, c show the variation of growth rate (αc_i) with α for the case $M = 3$, with $n = -1, -2, -3$ respectively. These results (and all those presented in this paper) are accurate to within the graphical accuracy of the figures. Because of the great multiplicity and close proximity of all these modes, we show the computed values of αc_i at each value of α. From the outset it should be stated that all our results relate to negative values of n; in general, we believe that instabilities are almost exclusively confined to this region of parameter space, with perhaps a few minor exceptions. We certainly expect the largest growth rates to be confined to the negative values of n (this is also the case when the flow is incompressible).

We see in figures 1 the following general trends: (i) an increase in growth rates as $-n$ increases; (ii) an apparent cut–off value of α above which no unstable modes exist; (iii) a

tendency for the maximum growth rate to be attained at an increasing value of α as $-n$ is increased; (iv) many modes of instability.

In figures 2 a, b, c, d, e, growth rates for the case $M = 5$ with $n = -1, -2, -3, -4, -5$ respectively are presented. The trends (i)—(iv) described above are again observed, together with the result that for corresponding n and α, the growth rates of $M = 5$ are substantially reduced compared to $M = 3$. Further the upper limit of α of the instability appears to be quite independent of M, and section 6 confirms this observation. Note that in figures 1 and 2, the lower range of α has been deliberately truncated. In this limit, our numerical results became extremely sensitive to grid size, and computation requirements became prohibitive.

These results suggest a number of interesting features, and in the following sections we mount a systematic study for increasing M, when $(-n) \gg 1$.

5. Asymptotic results, $(-n) \gg 1$

5.1 M=O(1)

It turns out that for this order of Mach number, to the orders to which we concern ourselves, the solution (in particular for the complex wavespeed) remains unchanged from the $-n \gg 1$ solution of the incompressible case, as considered by Leibovich & Stewartson (1983) and Duck (1986). However, since this solution forms a basis for the following subsections, we outline, briefly, the form of the structure in this case; full details can be found in the aforementioned papers. We have that

$$\alpha = n\bar{\alpha}, \quad \bar{\alpha} = O(1), \tag{5.1}$$

and the complex wavespeed develops as

$$c = c_0 + \frac{c_1}{n} + \frac{c_2}{|n|^{\frac{3}{2}}} + \dots \ . \tag{5.2}$$

Then generally

$$\varphi = n\varphi_0 + \varphi_1 + \frac{\varphi_2}{|n|^{\frac{1}{2}}} + \dots \ , \tag{5.3}$$

where

$$\varphi_0 = \bar{\alpha}(U(r) - c_0) + \frac{W(r)}{r}. \tag{5.4}$$

However the solution is found to be concentrated about points $r = r_0$ (critical points) where $\varphi_0(r = r_0) = 0$ and so

$$\bar{\alpha}(U(r_0) - c_0) + \frac{W(r_0)}{r_0} = 0. \tag{5.5}$$

However, it turns out that r_0 must in fact also be a turning point, and so

$$\varphi_0'(r_0) = 0, \tag{5.6}$$

i.e.

$$\bar{\alpha}U'(r_0) + \left(\frac{W}{r}\right)_0 = 0, \tag{5.7}$$

(where a subscript zero here and hereafter denotes evaluation at $r = r_0$). Equation (5.7) then serves to determine r_0, and hence c_0 may be determined from (5.5). The key length-scale inside the critical layer is given by

$$R = (r - r_0)|n|^{\frac{3}{4}}, \tag{5.8}$$

and then on this scale

$$\varphi = \varphi_1 - \frac{\text{sign}(n)}{|n|^{\frac{1}{2}}}\{-\bar{\alpha}c_2 + \frac{1}{2}\varphi_0''(r_0)R^2\} + \text{O}(n^{-1}), \tag{5.9}$$

where

$$\varphi_1 = -\bar{\alpha}c_1, \tag{5.10}$$

$$\varphi_0''(r_0) = \frac{d^2}{dr^2}[\varphi_0(r)]_{r=r_0}. \tag{5.11}$$

For consistency it was shown by Leibovich & Stewartson (1983) and Duck (1986) that

$$c_1^2 = \frac{(W^2r^2)_0'}{r_0^3\bar{\alpha}^2} - \frac{[(rW)_0' + \bar{\alpha}r_0^2U_0']^2}{(1+\bar{\alpha}^2r_0^2)r_0^2\bar{\alpha}^2}. \tag{5.12}$$

Further, on the $R = \text{O}(1)$ scale the eigenfunctions scale as

$$P = \overline{P} + \dots\ , \tag{5.13a}$$

$$G = n\overline{G} + \dots\ , \tag{5.13b}$$

and then $\overline{P}(R)$ is described by

$$\overline{P}_{RR} - \left\{2\left[\frac{c_2}{c_1} - \frac{\varphi_0''(r_0)R^2}{2\bar{\alpha}c_1}\right]\frac{\text{sign}(n)(1+\bar{\alpha}^2r_0^2)}{r_0^2}\right\}\overline{P} = 0, \tag{5.14}$$

or

$$\overline{P}_{\xi\xi} - \left\{\frac{1}{4}\xi^2 + \frac{\lambda_0 c_2}{2(\lambda_1)^{\frac{1}{2}}}\right\}\overline{P} = 0, \tag{5.15}$$

where we have written $\xi = 2^{\frac{1}{2}}\lambda_1^{\frac{1}{4}}R$, with

$$\lambda_0 = \frac{2}{c_1}\text{sign}(n)\frac{(1+\bar{\alpha}^2 r_0^2)}{r_0^2} \quad \text{and} \quad \lambda_1 = \frac{-\lambda_0\varphi_0''(r_0)}{2\bar{\alpha}}. \tag{5.16}$$

Equation (5.15) has a solution which may be written in terms of Weber parabolic cylinder functions, $D_m(\xi)$, and so if we demand the solution decays as $|\xi| \to \infty$, then m must be an integer, yielding the following result for c_2:

$$c_2 = -\frac{(\lambda_1)^{\frac{1}{2}}}{\lambda_0}(1+2m), \qquad m = 0, 1, 2, \ldots \tag{5.17}$$

Figure 3 shows the variation of growth rates for $M = 3$, for $n = -1$ (the least unstable mode shown) up to $n = -10$ (the most unstable mode shown) as computed for the full system; in all cases the most unstable mode for each value of n is shown. Using the asymptotic results above, we show the corresponding results in figure 4 (in particular we set $m = 0$ in (5.17)). The comparison between figures 3 and 4 reveals good agreement in the growth rates at larger values of $-n$, although at smaller values of $-n$, comparison is less good than the comparison of incompressible numerical and asymptotic results. This less satisfactory agreement may be attributed directly to the effects of compressibility, but for $|n|$ sufficiently large, the asymptotic results presented in this sub–section are ultimately approached.

In the following sub–section we begin to incorporate compressibility into our asymptotic description.

5.2 M=O($|n|^{\frac{1}{4}}$)

The key equation (5.14) was obtained by taking the O($|n|^{\frac{3}{4}}$) terms in equation (3.16). If $|n| \gg 1$, and we now permit M to grow in magnitude, additional terms will ultimately enter (5.14) when

$$M = |n|^{\frac{1}{4}}\widetilde{M}, \qquad \widetilde{M} = O(1), \tag{5.18}$$

when the coefficient of $\overline{P}$ will include the effects of compressibility. The modified equation is then

$$\overline{P}_{RR} - \mathrm{sign}(n)\Big\{2\Big[\frac{c_2}{c_1} - \frac{\varphi_0''(r_0)R^2}{2\bar{\alpha}c_1}\Big]\frac{(1+\bar{\alpha}^2 r_0^2)}{r_0^2} + \Big[\frac{(rW)_0' + \bar{\alpha}r_0^2 U_0'}{\bar{\alpha}c_1 r_0^2}\Big]\Big(\frac{W_0^2\widetilde{M}^2}{r_0}\Big)\Big\}\overline{P} = 0. \tag{5.19}$$

All other quantities (specifically c_0 and c_1) remain unchanged from those evaluated previously. This equation may be transformed to the same form as (5.15), viz

$$\overline{P}_{\xi\xi} - \Big\{\frac{1}{4}\xi^2 + \Big(\frac{\lambda_0 c_2 + \lambda_2)}{2(\lambda_1)^{\frac{1}{2}}}\Big\}\overline{P} = 0, \tag{5.20}$$

where λ_0 and λ_1 are given by (5.16), whilst

$$\lambda_2 = \mathrm{sign}(n)\left[\frac{(rW)_0' + \bar{\alpha}r_0^2 U_0'}{\bar{\alpha}r_0^2 c_1}\right]\left(\frac{W_0^2\widetilde{M}^2}{r_0}\right). \tag{5.21}$$

Consequently, using our previous arguments

$$c_2 = -\Big\{\frac{(\lambda_1)^{\frac{1}{2}}(1+2m) + \lambda_2}{\lambda_0}\Big\}, \qquad m = 0, 1, 2, \ldots \tag{5.22))}$$

Figure 5 shows a comparison of "exact" growth rates (obtained using the numerical approach of section 4), shown as a broken line, with the asymptotic results of this subsection; here, the chosen values of n are -5, -10 and -15 and we set $M = |n|^{\frac{1}{4}}$ i.e. $\widetilde{M} = 1$ in each case. The agreement is satisfactory, and improves as n increases. Figure 6 shows the corresponding comparison for c_r; in this case the agreement is excellent.

5.3 M=O($|n|^{\frac{3}{8}}$)

As M (and hence $\widetilde{M}$) increase in magnitude, the "λ_2 component" of c_2 increases (as $\widetilde{M}^2$) and becomes sufficiently larger than "λ_1 component". Simultaneously, the coefficient of P_r in (3.16) will grow, and further terms in the coefficient of P will become significant. The next important regime for M is when

$$M = |n|^{\frac{3}{8}}\widetilde{\widetilde{M}}, \qquad \widetilde{\widetilde{M}} = O(1). \tag{5.23}$$

Although the key radial scale remains $R = \mathrm{O}(1)$ (see (5.8)), the series development of c and $\varphi(R)$ is now altered, and is instead

$$c = c_0 + \frac{c_1}{n} + \frac{c_2}{|n|^{\frac{5}{4}}} + \frac{c_3}{|n|^{\frac{3}{2}}} + \dots \,, \tag{5.24}$$

and therefore,

$$\begin{aligned}\varphi &= \varphi_1 + \frac{\varphi_2}{|n|^{\frac{1}{4}}} + \frac{\varphi_3}{|n|^{\frac{1}{2}}} + \dots \\ &= -\bar{\alpha}c_1 - \frac{1}{|n|^{\frac{1}{4}}}\bar{\alpha}c_2 \mathrm{sign}(n) \\ &\qquad + \frac{1}{|n|^{\frac{1}{2}}}\Big\{-\bar{\alpha}c_3 \mathrm{sign}(n) + \frac{1}{2}\varphi_0''(r_0)R^2\Big\} + \dots \,.\end{aligned} \tag{5.25}$$

Considering $\mathrm{O}(|n|^{\frac{7}{4}})$ quantities in (3.16) requires that the sum of these terms is zero, and so this leads to,

$$c_2 = -\mathrm{sign}(n)\frac{\widetilde{\widetilde{M^2}}W_0^2}{2\bar{\alpha}r_0}\Big[\frac{(rW)_0' + \bar{\alpha}r_0^2 U_0'}{1+\bar{\alpha}^2 r_0^2}\Big]. \tag{5.26}$$

The equation for $\overline{P}(R)$ is again obtained by taking the $\mathrm{O}(|n|^{\frac{3}{2}})$ terms in (3.16), namely

$$\overline{P}_{RR} - \frac{\widetilde{\widetilde{M^2}}W_0^2}{r_0}\overline{P}_R - \Big\{\frac{1+\bar{\alpha}^2 r_0^2}{r_0^2}\Big[2\frac{\varphi_3}{\varphi_1} + \frac{\varphi_2^2}{\varphi_1^2}\Big]\Big\}\overline{P} = 0. \tag{5.27}$$

Using the standard transformation

$$\overline{P}(R) = \overline{P}^*(R)\exp\Big[\frac{1}{2}\frac{\widetilde{\widetilde{M^2}}W_0^2 R}{r_0}\Big], \tag{5.28}$$

then

$$\begin{aligned}\overline{P}^*_{RR} - \Big\{2\ \mathrm{sign}(n)\Big(\frac{c_3}{c_1} - \frac{\varphi_0''(r_0)R^2}{2\bar{\alpha}c_1}\Big)\Big(\frac{1+\bar{\alpha}^2 r_0^2}{r_0^2}\Big) \\ + \Big(\frac{\widetilde{\widetilde{M^2}}W_0^2}{2r_0}\Big)^2\Big\}\overline{P}^* = 0,\end{aligned} \tag{5.29}$$

or

$$\overline{P}^*_{\xi\xi} - \left[\frac{1}{4}\xi^2 + \frac{\lambda_0 c_2 + \lambda_3}{2(\lambda_1)^{\frac{1}{2}}}\right]\overline{P}^* = 0, \tag{5.30}$$

where

$$\lambda_3 = \left[\frac{\widetilde{\widetilde{M}}^2 W_0^2}{2r_0}\right]^2. \tag{5.31}$$

Since (5.30) is again a form of Weber's equation, then

$$c_3 = -\left\{\frac{(\lambda_1)^{\frac{1}{2}}(1+2m) + \lambda_3}{\lambda_0}\right\}, \qquad m = 0, 1, 2, \ldots \tag{5.32}$$

Figure 7 shows a comparison of asymptotic results (solid lines) with numerical results (broken line), for n =-5, -10, -15 with $M = |n|^{\frac{3}{8}}$ (i.e. $\widetilde{\widetilde{M}} = 1$). Again the comparison becomes markedly better as $|n|$ increases. The corresponding distribution of c_r is again good, and shown in figure 8.

5.4 M=O($|n|^{\frac{1}{2}}$)

In this case it is quite clear from the previous subsection that when $\widetilde{\widetilde{M}} = \mathrm{O}(|n|^{\frac{1}{8}})$, then the c_2 term (see (5.26)), which grows as $\widetilde{\widetilde{M}}^2$ will become comparable in magnitude to the term involving c_1 (which is independent of $\widetilde{\widetilde{M}}$); in addition to this, since c_3 grows as $\widetilde{\widetilde{M}}^4$ as $\widetilde{\widetilde{M}}$ increases, then this term will also become comparable to the c_1 term when $M = \mathrm{O}(|n|^{\frac{1}{2}})$. In this case, it is straightforward to show that $R = \mathrm{O}(1)$ remains the appropriate radial scale, whilst the wavespeed expands as follows

$$c = c_0 + \frac{c_1}{n} + \frac{c_2}{|n|^{\frac{3}{2}}} + \ldots\ , \tag{5.33}$$

implying

$$\varphi = \varphi_1 + \frac{\varphi_2}{|n|^{\frac{1}{2}}} + \ldots\ . \tag{5.34}$$

If we write

$$M = |n|^{\frac{1}{2}}\widehat{M}, \qquad \widehat{M} = O(1), \tag{5.35}$$

then the equation for $\overline{P}(R)$ is

$$\overline{P}_{RR} - \Big\{|n|^{\frac{1}{2}}\Big[\Big(\frac{(rW)_0' + \bar{\alpha}r_0^2U_0'}{r_0^2\varphi_1}\Big)\Big(\frac{2W_0}{r_0^2\varphi_1} - \mathrm{sign}(n)\frac{\widehat{M}^2W_0^2}{r_0}\Big) + \Big(\frac{1+\bar{\alpha}^2r_0^2}{r_0^2\varphi_1}\Big)\Big(\varphi_1 - \frac{(W^2r^2)_0'}{r_0^3\varphi_1}\Big)\Big] + \Big[-2\Big(\frac{(rW)_0' + \bar{\alpha}r_0^2U_0'}{r_0^2\varphi_1}\Big)^2\frac{\varphi_2}{\varphi_1} + \mathrm{sign}(n)\Big(\frac{(rW)_0' + \bar{\alpha}r_0^2U_0'}{r_0^2\varphi_1}\Big)\Big(\frac{\widehat{M}^2W_0^2}{r_0}\Big)\frac{\varphi_2}{\varphi_1} + 2\Big(\frac{1+\bar{\alpha}^2r_0^2}{r_0^2\varphi_1}\Big)\Big(\frac{(W^2r^2)_0'}{r_0^2\varphi_1}\Big)\frac{\varphi_2}{\varphi_1}\Big]\Big\}\overline{P}^* = 0. \tag{5.36}$$

Again using a standard transformation of the form

$$\overline{P}(R) = \overline{P}(R)\exp\Big[\frac{1}{2}\frac{|n|^{\frac{1}{4}}\widehat{M}^2W_0^2R}{r_0}\Big], \tag{5.37}$$

leads to the differential equation

$$\overline{P}_{RR} - \Big\{|n|^{\frac{1}{2}}\Big[\Big(\frac{(rW)_0' + \bar{\alpha}r_0^2U_0'}{r_0^2\varphi_1}\Big)\Big(\frac{2W_0}{r_0^2\varphi_1} - \mathrm{sign}(n)\frac{\widehat{M}^2W_0^2}{r_0}\Big) + \Big(\frac{1+\bar{\alpha}^2r_0^2}{r_0^2\varphi_1}\Big)\Big(\varphi_1 - \frac{(W^2r^2)_0'}{r_0^3\varphi_1}\Big) + \Big(\frac{\widehat{M}^2W_0^2}{2r_0}\Big)^2\Big] + \Big[-2\Big(\frac{(rW)_0' + \bar{\alpha}r_0^2U_0'}{r_0^2\varphi_1}\Big)^2\frac{\varphi_2}{\varphi_1} + \mathrm{sign}(n)\Big(\frac{(rW)_0' + \bar{\alpha}r_0^2U_0'}{r_0^2\varphi_1}\Big)\Big(\frac{\widehat{M}^2W_0^2}{r_0}\Big)\frac{\varphi_2}{\varphi_1} + 2\Big(\frac{1+\bar{\alpha}^2r_0^2}{r_0^2\varphi_1}\Big)\Big(\frac{(W^2r^2)_0'}{r_0^2\varphi_1}\Big)\frac{\varphi_2}{\varphi_1}\Big]\Big\}\overline{P}^* = 0. \tag{5.38}$$

If our assumption regarding the importance of the $R = \mathrm{O}(1)$ scale is to be consistent, (although see the comments below regarding $R = \mathrm{O}(|n|^{\frac{1}{4}})$) then the coefficient involving

$|n|^{\frac{1}{2}}$ above, must be zero. (This is also consistent with the previous smaller orders of Mach number considered previously). This leads to

$$c_1 = \frac{-\frac{\widehat{M}^2 W_0^2}{2\bar{\alpha} r_0}\Big(\frac{(rW)_0' + \bar{\alpha} r_0^2 U_0'}{1+\bar{\alpha}^2 r_0^2}\Big) \pm \sqrt{\Big(\frac{\widehat{M}^2 W_0^2}{2\bar{\alpha} r_0^2}\Big)^2 \frac{(W^2 r^2)_0' r_0}{1+\bar{\alpha}^2 r_0^2} + c_1^{\mathrm{inc}\,2}}}{1 + \frac{1}{1+\bar{\alpha}^2 r_0^2}\Big(\frac{\widehat{M}^2 W_0^2}{2}\Big)^2}, \tag{5.39}$$

where c_1^{inc} denotes the incompressible value of c_1, given by (5.12). The equation that determines $\overline{P}(R)$ is then,

$$\overline{P}^*_{RR} - \Big\{2\Big(\frac{c_2}{c_1} - \frac{\varphi_0''(r_0)R^2}{2\bar{\alpha}c_1}\Big)\mathrm{sign}(n)\Big[\frac{1+\bar{\alpha}^2 r_0^2}{r_0^2} + \Big(\frac{\widehat{M}^2 W_0^2}{2r_0}\Big)^2$$

$$+\mathrm{sign}(n)\frac{W_0^2 \widehat{M}^2}{2r_0}\Big(\frac{(rW)_0' + \bar{\alpha} r_0^2 U_0'}{r_0^2 \bar{\alpha} c_1}\Big)\Big]\Big\}\overline{P}^* = 0, \tag{5.40}$$

or symbolically

$$\overline{P}^*_{RR} - [\hat{\lambda}_1 R^2 + \hat{\lambda}_0 c_2]\overline{P}^* = 0, \tag{5.41}$$

and using previous arguments, we must have

$$c_2 = -\frac{(\hat{\lambda}_1)^{\frac{1}{2}}(1+2m)}{\hat{\lambda}_0} \qquad m = 0, 1, 2 \ldots \ . \tag{5.42}$$

Note that although the transformation (5.37) suggests growth as $R \to \infty$, this is more than offset by the decay of the parabolic cylinder functions, albeit on a larger lengthscale $R = \mathrm{O}(|n|^{\frac{1}{4}})$. Note too that the transformation (5.37) is consistent with that used previously, namely (5.28).

Figure 9 shows comparison between the above asymptotic results (solid line) and the "exact" numerical results (broken line), for the most unstable growth rates when n = -5, -10, -15 ($M = |n|^{\frac{1}{2}}$, i.e. $\widehat{M} = 1$ in all cases). Again the agreement is seen to improve as $-n$ increases. Figure 10 shows a comparison between the corresponding c_r's, for the above cases and indicates good agreement between our asymptotic and numerical results.

It turns out, however, that this order of M marks a watershed. When $\widehat{M}$ is not large, both roots of c_1 must be complex (and from our previous discussions, the flow is unstable). As $\widehat{M}$ increases, however, eventually terms inside the square root term in (5.39) will eventually become positive, and hence the two roots of c_1 will cease to be complex conjugate pairs, but will both become real. In particular, this will occur when

$$\frac{\widehat{M}_\infty^2 W_0^2}{2\bar{\alpha} r_0^2} \frac{(W^2 r^2)_0' r_0}{1+\bar{\alpha}^2 r_0^2} = c_1^{inc^2}. \tag{5.43}$$

To illustrate the stabilisation of these modes, in figures 11 a, b, c, we show the variation of the growth rates with M for the cases $n = -5$ and $\alpha = 2.5$, $n = -10$ and $\alpha = 5$, $n = -15$ and $\alpha = 7.5$ respectively. We clearly see these modes becoming neutrally stable at finite values of M. For comparison, in figures 12a—12c (corresponding to figures 11a—11c respectively) we show the corresponding results from solutions of the full system (3.11), (3.12). At the lower values of M, there is good correlation between the two sets of results. However, as the Mach number increases, and as the order of the modes (i.e. m) increases, the correlation deteriorates. We consider this latter point first by examining the behaviour of the higher order modes.

5.5 The structure when m =O($|n|^{\frac{1}{2}}$) , (M=O($|n|^{\frac{1}{2}}$))

One detail that has not been considered so far, is the behaviour of the modes as m increases. This feature was considered by Duck (1986), and we consider this aspect here, for the important case when $M = O(|n|^{\frac{1}{2}})$. c develops in the same manner as in the previous sub–section, and close to the critical layer φ takes the form

$$\varphi = \varphi_1 + \frac{1}{|n|^{\frac{1}{2}}}\varphi_2 + \dots . \tag{5.44}$$

c_0 remains unchanged from that given previously, however c_1 will differ. In this case, we consider the lengthscale

$$\widetilde{R} = (r - r_0)|n|^{\frac{1}{2}} = O(1), \tag{5.45}$$

and so on this scale

$$\varphi_1 = -\bar{\alpha}c_1 + \frac{\text{sign}(n)}{2}\varphi_0''(r_0)\widetilde{R}^2, \tag{5.46}$$

$$\varphi_2 = -\bar{\alpha}c_2 + \frac{\text{sign}(n)}{3!}\varphi_0'''(r_0)\widetilde{R}^3. \tag{5.47}$$

Substitution of these expansions into our governing equation gives, to leading order, an eigenfunction equation of the form

$$P_{\widetilde{R}\widetilde{R}} + q_1(\widetilde{R})P_{\widetilde{R}} + |n|q_2(\widetilde{R})P = 0. \tag{5.48}$$

Using the standard transformation

$$P(\widetilde{R}) = P^*(\widetilde{R})exp\Big[-\frac{1}{2}\int q_1(\widetilde{R})d\widetilde{R}\Big], \tag{5.49}$$

we obtain

$$P^*_{\widetilde{R}\widetilde{R}} + \big[|n|q_2 - \frac{1}{2}q_{1\widetilde{R}} - \frac{1}{4}q_1^2\big]P^* = 0. \tag{5.50}$$

However, since $|n|$ is large, (5.50) may be approximated by

$$P^*_{\widetilde{R}\widetilde{R}} + |n|q_2P^* = 0, \tag{5.51}$$

where

$$q_2 = -\frac{1}{r_0^5\varphi_1^2}\Big[4r_0W_0^2 + (1+\bar{\alpha}^2r_0^2)\big(r_0^3\varphi_1^3 - (W^2r^2)_0'\big) \\ -\text{sign}(n)2W_0^2r_0^2\widehat{M}^2\varphi_1 + \frac{\widehat{M}^4W_0^4\varphi_1^2r_0^3}{4}\Big]. \tag{5.52}$$

Thus (5.50) may be written as

$$P^*_{\tilde{\xi}\tilde{\xi}} + h^2\Big[\frac{\mu}{(1+\tilde{\xi}^2)^2} - \frac{\eta}{(1+\tilde{\xi}^2)} - \nu\Big]P^* = 0, \tag{5.53}$$

with

$$\mu = \frac{2[4r_0 W_0^2 - (1+\bar{\alpha}^2 r_0^2)(W^2 r^2)_0'] \text{sign}(n)}{\bar{\alpha} c_1 r_0^2 \varphi_0''(r_0)}, \tag{5.54}$$

$$\nu = \frac{-2[(1+\bar{\alpha}^2 r_0^2) + \widehat{M}^4 W_0^4/4]\bar{\alpha} c_1 \text{sign}(n)}{r_0^2 \varphi_0''(r_0)}, \tag{5.55}$$

$$\eta = \frac{4 W_0^3 \widehat{M}^2}{r_0^3 \varphi_0''(r_0)}, \tag{5.56}$$

$$\tilde{\xi} = \left[\frac{-\varphi_0''(r_0)\text{sign}(n)}{2\bar{\alpha} c_1}\right]^{\frac{1}{2}} \widetilde{R}, \tag{5.57}$$

$$h^2 = |n|. \tag{5.58}$$

Equation (5.53) is now in a form suitable for a WKBJ type of approximation. This equation has four turning points, however for the range of $\tilde{\xi}$ required that we need consider only the turning points at

$$\tilde{\xi} = \pm\left[-\frac{1}{2}\frac{\eta}{\nu} + \frac{1}{2}\sqrt{\frac{\eta^2}{\nu^2} + \frac{4\mu}{\nu}} - 1\right]^{\frac{1}{2}} \tag{5.59}$$

For large h the WKBJ solution is given by

$$P^* = \tilde{q}^{-\frac{1}{4}}\left[A_1 \exp\int (ih\tilde{q}^{\frac{1}{2}} d\tilde{\xi}) + A_2 \exp\int -(ih\tilde{q}^{\frac{1}{2}} d\tilde{\xi})\right], \tag{5.60}$$

where

$$\tilde{q} = \frac{\mu}{(1+\tilde{\xi}^2)^2} - \frac{\eta}{(1+\tilde{\xi}^2)} - \nu. \tag{5.61}$$

The treatment near the turning points is standard (see for example Duck 1986) and leads to the following dispersion relationship for c_1

$$Ih = -\frac{\pi}{4}(1+2m), \quad m = 0, 1, 2, \ldots \tag{5.62}$$

where

$$I = \int_{\tilde{\xi}_1}^{0} \left\{ \frac{\mu}{(1+\tilde{\xi}^2)^2} - \frac{\eta}{(1+\tilde{\xi}^2)} - \nu \right\}^{\frac{1}{2}} d\tilde{\xi}$$

$$= \nu^{\frac{1}{2}} g \left\{ -\left(\frac{1}{2}g - \frac{\eta}{2\nu}\right) F\left(\frac{\pi}{2}, k\right) + g_1 E\left(\frac{\pi}{2}, k\right) \right.$$

$$\left. -\frac{\mu}{\nu}\left(\frac{1}{(-\frac{1}{2}\frac{\eta}{\nu} + \frac{1}{2}g_1}\right) \Pi\left(\frac{\pi}{2}, \widehat{\alpha}^2, k\right) \right\}, \tag{5.63}$$

$$\tilde{\xi}_1 = \left[-\frac{1}{2}\frac{\eta}{\nu} + \frac{1}{2}\sqrt{\frac{\eta^2}{\nu^2} + \frac{4\mu}{\nu}} - 1 \right]^{\frac{1}{2}}, \tag{5.64}$$

$$g = \frac{1}{i(\frac{\eta^2}{\nu^2} + \frac{4\mu}{\nu})^{1/4}}, \tag{5.65}$$

$$g_1 = \frac{1}{g^2}, \tag{5.66}$$

$$k = g\left(-\frac{\eta}{2\nu} + \frac{1}{2}g_1 - 1\right)^{\frac{1}{2}}, \tag{5.67}$$

$$\widehat{\alpha}^2 = \frac{-2k^2}{(\frac{\eta}{\nu} - g_1)g^2}. \tag{5.68}$$

Here, $F(\frac{\pi}{2}, k)$, $E(\frac{\pi}{2}, k)$, $\Pi(\frac{\pi}{2}, \widehat{\alpha}^2, k)$ denote complete elliptic integrals of the first, second and third kinds respectively.

The system (5.62) was solved using Newton iteration, and results for variations of growth rate with M were computed for $m = 0, 1, 2, 3, 4, 5$ for the cases $n = -5, \alpha = 2.5$ (figure 13a), $n - 10, \alpha = 5$ (figure 13b), $n = -15, \alpha = 7.5$ (figure 13c). The modified theory of this subsection does indicate some important improvement in the comparison with figures 12; in particular the "bunching up" of the modes with an increase in order is captured. However, although for $n = -15$ there is quite good correlation for the lower order modes, as m increases, the various wiggles observed in figures 12 are not described, and more importantly our asymptotic results do not capture the instability shown in figures 12

beyond about $M = 8$. Indeed, figure 12 indicates instability as $\widehat{M}$ increases. We therefore conclude that the nature of these modes, as $\widehat{M} \to \infty$ is somewhat different. It turns out from the analysis of the following section that as $\widehat{M} \to \infty$, a further class of mode emerges, quite distinct from those considered so far.

6. Centre Modes, M=O(|n|)

Here we examine modes exhibited when the Mach number is of order n, i.e.

$$M = |n|\overline{M}, \quad \overline{M} = \mathrm{O}(1). \tag{6.1}$$

As noted previously, as $M \to \infty$, the features of the modes exhibited at lower Mach numbers cease to exist. In fact the analysis of sub–section 5.5 suggests that the modes in this regime under present consideration are neutral. However, our numerics belie this and point towards the existence of *centre modes*, by which we mean, the eigenvalues are determined primarily by conditions close to the axis of the vortex, $r = 0$, in a manner similar to that of Stewartson and Brown (1984, 1985). Here, the complex wavespeed develops as

$$c = c_0 + \frac{c_1}{n^2} + \dots \ , \tag{6.2}$$

(an expansion that can be verified a *posteriori*) and therefore

$$\begin{aligned} \varphi &= n\varphi_0 + \frac{\varphi_1}{n} + \dots \\ &= n\Big\{\bar{\alpha}(U - c_0) + \frac{W}{r}\Big\} + \Big\{-\bar{\alpha}c_1 + \frac{1}{2n}\varphi_0''(0)r^2\Big\} + \dots \end{aligned} \tag{6.3}$$

In order to be consistent we must have that $\varphi_0(r = 0) = 0$, i.e.

$$c_0 = 1 + \frac{q}{\bar{\alpha}}. \tag{6.4}$$

We must now go on to find c_1 in our complex wavespeed expansion. The solutions are, in the main, trapped in the region around $r = 0$, but we begin by showing how these solutions are connected to the outer flow. The flow is divided into the four regions, which are considered in turn.

We first begin our analysis at the outer region of the flow, where $r = O(1)$, and the governing equation has the form

$$P_{rr} - |n|^2 \frac{W^2\overline{M}^2}{r} P_r + |n|^4 \overline{M}^2 \varphi_0^2 P = 0. \tag{6.5}$$

Using a transformation of the form

$$P = P^*(r)\exp\left\{\int_{\tilde{r}_0}^{r} \frac{n^2 W^2 \widehat{M}^2}{2r} dr\right\}, \tag{6.6}$$

and writing

$$\chi_0 = -\widehat{M}^2\varphi_0^2 + \frac{W^4\overline{M}^4}{4r^2}, \tag{6.7}$$

reduces (6.5) to

$$P^*_{rr} - |n|^4\chi_0 P^* = 0. \tag{6.8}$$

We define the critical point $\tilde{r}_0$ by $\chi_0(\tilde{r}_0) = 0$ and when $r > \tilde{r}_0$, $\chi_0 < 0$ and the approximate solution to (6.8) is given by

$$P^* = \frac{E_1}{[-\chi_0]^{\frac{1}{4}}}\exp\left\{i|n|^2\int_{\tilde{r}_0}^{r}[-\chi_0]^{\frac{1}{2}}dr\right\}, \tag{6.9}$$

where E_1 is an unknown constant.

We have also assumed that $[-\chi_0]^{\frac{1}{2}}$ is slightly imaginary, with its imaginary part positive. This condition is to ensure that the solution is bounded as $r \to \infty$, otherwise if $Im\{[-\chi_0]^{\frac{1}{2}}\} < 0$ we replace 'i' by '$-i$' in (6.9). Looking at this point from a more physical perspective, we require waves to propagate out from the critical layer and not in toward it.

In order to be able to match (6.9) with the solution in the $r < \tilde{r}_0$ region, we must first examine the solution of the flow in the transition layer, around $r = \tilde{r}_0$. The lengthscale in this region turns out to be

$$r - \tilde{r}_0 = \widehat{R}|n|^{-\frac{4}{3}}, \quad \widehat{R} = \mathrm{O}(1), \tag{6.10}$$

and use of this scaling reduces our governing equation to the Airy equation, which has solutions of the form

$$P^* = F_1\mathrm{Ai}(\chi_0'(\tilde{r}_0))^{\frac{1}{3}}\widehat{R}) + F_2\mathrm{Bi}(\chi_0'(\tilde{r}_0))^{\frac{1}{3}}\widehat{R}). \tag{6.11}$$

Standard analysis and matching with (6.9) yields the result

$$F_1 = iF_2. \tag{6.12}$$

In the region $r < \tilde{r}_0$, $\chi_0 > 0$ and hence the WKBJ solution here is given by

$$P^* = \frac{1}{\chi_0^{\frac{1}{4}}}\Bigg\{D_1 \exp\Big\{\int_{\tilde{r}_0}^{r} |n|^2\Big[\frac{W^4\overline{M}^4}{4r^2} - \overline{M}^2\varphi_0^2\Big]^{\frac{1}{2}} dr\Big\}$$

$$+D_2 \exp\Big\{-\int_{\tilde{r}_0}^{r} |n|^2\Big[\frac{W^4\overline{M}^4}{4r^2} - \overline{M}^2\varphi_0^2\Big]^{\frac{1}{2}} dr\Big\}\Bigg\}. \tag{6.13}$$

As we approach the transition–layer this solution must match with (6.11) implying

$$D_1 = -iD_2\sqrt{3}. \tag{6.14}$$

Note that as $r \to 0$

$$P^* \sim \frac{2^{\frac{1}{2}}}{q\overline{M}r^{\frac{1}{2}}}\Bigg\{D_1 Z_1 \exp\Big(\frac{q^2\overline{M}^2 r^2|n|^2}{4}\Big) + D_2 Z_2 \exp\Big(-\frac{q^2\overline{M}^2 r^2|n|^2}{4}\Big)\Bigg\}, \tag{6.15}$$

where,

$$Z_1 = \exp\Bigg\{\int_{\tilde{r}_0}^{0} |n|^2\Big(\chi_0^{\frac{1}{2}} - \frac{q^2\overline{M}^2 r}{2}\Big)dr\Bigg\}, \tag{6.16}$$

$$Z_2 = \frac{1}{Z_1}. \tag{6.17}$$

We now consider the lengthscale, $r = \mathrm{O}(|n|^{-\frac{1}{2}})$, by setting

$$\bar{r} = r|n|^{\frac{1}{2}} = \mathrm{O}(1). \tag{6.18}$$

The governing equation in this region, to leading order, is given by

$$P_{\bar{r}\bar{r}} - |n|q^2\overline{M}^2\bar{r}P_{\bar{r}} + |n|^2\Big[\frac{2q^3\overline{M}^2}{\varphi_1} - \frac{1}{\bar{r}^2}\Big]P = 0, \tag{6.19}$$

where

$$\varphi_1 = \frac{1}{2}\varphi_0''(0)\bar{r}^2, \tag{6.20}$$

and as previously, it is necessary to use a transformation, which is of the standard type, i.e.

$$P = P^{**}\exp\Big\{\frac{1}{2}\int |n|q^2\bar{r}\overline{M}d\bar{r}\Big\}, \tag{6.21}$$

which leads to the final form of the governing equation in this region, viz

$$P^{**}_{\bar{r}\bar{r}} + |n|^2\left[\frac{2q^3\overline{M}^2}{\frac{1}{2}\varphi_0''(0)\bar{r}^2} - \frac{1}{\bar{r}^2} - \frac{q^4\bar{r}^2\overline{M}^4}{4}\right]P^{**} = 0. \tag{6.22}$$

This equations yields solutions of the form

$$P^{**} = \bar{r}^{\frac{1}{2}}\Big(C_1 I_\nu(\frac{q^2\overline{M}^2|n|\bar{r}^2}{4}) + C_2 K_\nu(\frac{q^2\overline{M}^2|n|\bar{r}^2}{4})\Big), \tag{6.23}$$

where I and K are modified Bessel functions, written in standard form, with

$$\nu = \frac{|n|}{2}\Big(1 - \frac{2q^3\overline{M}^2}{\frac{1}{2}\varphi_0''(0)}\Big)^{\frac{1}{2}}. \tag{6.24}$$

Now, as $\bar{r} \to \infty$

$$P^{**} \sim \frac{C_1\bar{r}^{\frac{1}{2}}}{\sqrt{2\pi q^2\overline{M}^2|n|\bar{r}^2/4}}\exp\Big(\frac{q^2\overline{M}^2|n|\bar{r}^2}{4}\Big)$$

$$+C_2\bar{r}^{\frac{1}{2}}\sqrt{\frac{\pi}{2q^2\overline{M}^2|n|\bar{r}^2/4}}\exp\Big(-\frac{q^2\overline{M}^2|n|\bar{r}^2}{4}\Big), \tag{6.25}$$

and comparing this with equation (6.15), we see that in order for these solutions to match and taking into account equation (6.14), then

$$C_1 = -i\pi\sqrt{3}Z_1^2C_2. \tag{6.26}$$

Also, we take note of the fact that as $\bar{r} \to 0$, then

$$P^{**} \sim \bar{r}^{\frac{1}{2}} \Big(\frac{C_1 (\frac{1}{2}\beta_1 \bar{r}^2)^{\nu}}{\Gamma(\nu+1)} + \frac{C_2}{2} \Gamma(\nu) \Big(\frac{1}{2}\beta_1 \bar{r}^2 \Big)^{-\nu} \Big), \tag{6.27}$$

where $\beta_1 = q^2 \overline{M}^2 |n|/4$ and $\Gamma(\nu)$ is the gamma function, defined in the standard fashion. Next we set

$$R = r|n| = \mathrm{O}(1), \tag{6.28}$$

and in this regime φ develops as

$$\begin{aligned} \varphi &= \frac{\varphi_1}{n} + \dots \\ &= \frac{1}{n} \Big(-\bar{\alpha} c_1 + \frac{1}{2} \varphi_0''(0) R^2 \Big) + \dots \ , \end{aligned} \tag{6.29}$$

with the governing equation

$$P_{RR} + |n|^2 \Big[\frac{4\bar{\alpha}^2 q^2 + 4\bar{\alpha} q}{[-\bar{\alpha} c_1 + \frac{1}{2}\varphi_0''(0) R^2]^2} + \frac{2q^3 \overline{M}^2}{[-\bar{\alpha} c_1 + \frac{1}{2}\varphi_0''(0) R^2]} - \frac{1}{R^2} \Big] P = 0, \tag{6.30}$$

which has the solution

$$P = \frac{(\Upsilon R^2)^{\frac{|n|}{2} + \frac{1}{4}}}{(1 - \Upsilon R^2)^{\hat{\mu}}} F(\varpi_1; \varpi_2; |n| + 1; \Upsilon R^2), \tag{6.31}$$

where, F is the hypergeometric function in standard notation, and

$$\Upsilon = \frac{\frac{1}{2}\varphi_0''(0)}{\bar{\alpha} c_1}, \tag{6.32a}$$

$$\varpi_1 = \frac{1}{2}(|n| - s) - \hat{\mu}, \tag{6.32b}$$

$$\varpi_2 = \frac{1}{2}(|n| + s) - \hat{\mu}, \tag{6.32c}$$

$$s = (|n|^2 + b)^{\frac{1}{2}}, \tag{6.32d}$$

$$\hat{\mu}(\hat{\mu} + 1) = -\frac{a\Upsilon}{4}, \tag{6.32e}$$

with

$$a = |n|^2 \left\{ \frac{4q\bar{\alpha} + 4q^2\bar{\alpha}^2}{\frac{1}{4}\left(\varphi_0''(0)\right)^2} \right\}, \tag{6.33a}$$

$$b = -\frac{4q^3|n|^2\overline{M}^2}{\varphi_0''(0)}. \tag{6.33b}$$

Note that this equation is very similar in form to that found by Stewartson & Capell (1985). This solution is of course finite at $R = 0$ by the definition of the hypergeometric function, and therefore satisfies our boundary conditions at the centre of the vortex. As R becomes large

$$P \sim R^{\frac{1}{2}}(A_1 R^s + A_2 R^{-s}), \tag{6.34}$$

matching this with (6.27) and making use of (6.26) we see that,

$$\frac{\Gamma(s/2+1)\Gamma(s/2)|n|^s}{(\frac{1}{2}\beta_1)^s Z_1^2} A_1 = -i\pi A_2 2\sqrt{3}, \tag{6.35}$$

which gives us a relationship between A_1 and A_2. We now go on to determine c_1 explicitly.

We begin, by writing P, as $R \to \infty$, in terms of its asymptotic expansion in this limit, i.e.

$$P \sim \frac{(\Upsilon R^2)^{\frac{|n|}{2}+\frac{1}{4}}}{(1-\Upsilon R^2)^{\hat{\mu}}} \left[\varsigma_0 (-\Upsilon R^2)^{\hat{\mu}-\frac{|n|}{2}+\frac{s}{2}} \sum\nolimits_1 + \delta_0 (-\Upsilon R^2)^{\hat{\mu}-\frac{|n|}{2}-\frac{s}{2}} \sum\nolimits_2 \right], \tag{6.36}$$

where,

$$\varsigma_0 = \frac{|n|!\,(s-1)!}{\left(\frac{|n|}{2}+\frac{s}{2}-\hat{\mu}-1\right)!\left(\frac{|n|}{2}+\frac{s}{2}+\hat{\mu}\right)!}, \tag{6.37a}$$

$$\delta_0 = \frac{|n|!\,(-s-1)!}{\left(\frac{|n|}{2}-\frac{s}{2}-\hat{\mu}-1\right)!\left(\frac{|n|}{2}-\frac{s}{2}+\hat{\mu}\right)!}, \tag{6.37b}$$

and $\sum_1$ and $\sum_2$ are both power series expansions in $1/\Upsilon R^2$, with their leading order terms unity. Matching the two large R solutions, (6.34) and (6.36) yields the relationship,

$$\frac{A_1}{A_2} = \frac{\varsigma_0}{\delta_0}(-\Upsilon)^s. \tag{6.38}$$

However, since $|s| \gg 0$ then $|\Upsilon^s| \gg 0$, which in turn implies that $|\varsigma_0| \gg |\delta_0|$, and therefore to leading order, $\varsigma_0 = 0$. Hence, we see that, $\frac{1}{2}(|n| + s) - \hat{\mu}$ must be either a negative integer or zero, i.e.

$$\hat{\mu}_0 = \frac{1}{2}(|n| + s) + N, \qquad (N \geq 0), \tag{6.39}$$

for integer N, where $\hat{\mu}_0$ denotes a first order approximation to $\hat{\mu}$.

Since s is imaginary, the above expression substituted into (6.32e) and (6.32a) gives the leading order imaginary contribution to c_1. i.e. it is obtained from

$$c_1 = -\frac{a\phi_0''(0)}{8\bar{\alpha}\hat{\mu}_0(\hat{\mu}_0 + 1)}. \tag{6.40}$$

It is also possible to obtain the correction to this term by retaining the next order approximation to μ. On setting, $\hat{\mu} = \hat{\mu}_0 + \Delta\hat{\mu}$, where $|\Delta\hat{\mu}| \ll 1$, then we obtain

$$\varsigma_0 = \frac{(-1)^{N+1}|n|!\,N!\,(s-1)!}{(s + |n| + N)!}\Delta\hat{\mu}, \tag{6.41a}$$

$$\delta_0 = \frac{(-1)^N|n|!\,(s+N)!}{s!\,(|n| + N)!}, \tag{6.41b}$$

and then (6.38) gives

$$\Delta\hat{\mu} = -\frac{A_1}{A_2}(-\Upsilon)^{-s}\frac{(s + |n| + N)!\,(s+N)!}{s!\,(s-1)!\,N!\,(|n| + N)!}. \tag{6.42}$$

Since

$$\hat{\mu}(\hat{\mu} + 1) = -\frac{\frac{1}{2}a\varphi_0''(0)}{4\bar{\alpha}c_1}, \tag{6.43}$$

and therefore, if we allow $\hat{\mu} = \hat{\mu}_0 + \Delta\hat{\mu}$ in the above, we see that

$$c_1 = -\frac{a\varphi_0''(0)}{8\bar{\alpha}\hat{\mu}_0(\hat{\mu}_0+1)}\left(1 - \frac{(2\hat{\mu}_0+1)}{4\hat{\mu}_0(\hat{\mu}_0+1)}\Delta\hat{\mu}\right). \tag{6.44}$$

Therefore, we may now write c_1 as

$$c_1 = -\frac{a\varphi_0''(0)}{8\bar{\alpha}\hat{\mu}_0(\hat{\mu}_0+1)}\left[1 + \frac{A_1}{A_2}\left(\frac{a}{4\hat{\mu}_0(\hat{\mu}_0+1)}\right)^s \frac{(s+|n|+N)!\,(s+N)!}{s!\,(s-1)!\,N!\,(|n|+N)!}\right.$$

$$\left. \times \frac{(2\hat{\mu}_0+1)}{4\hat{\mu}_0(\hat{\mu}_0+1)}\right], \tag{6.45}$$

where, all variables in this expression have been previously defined. However, the correction term is found to be of several orders of magnitude smaller than the leading order term of c_1.

In figure 14a we show the variation of the growth rate with α for the case $n = -5$, $M = 5$. This figure is to be compared with figure 2e, computed from the full system; comparison between the asymptotic and fully numerical results is surprisingly good, considering the smallness of $-n$ and M. Figures 14b shows the growth rate variation, predicted from the analysis of this subsection, for the case $n = -10$, $M = 10$ and is to be compared with the fully numerical results shown in figure 15. Again, the results are encouraging, in particular the magnitude and location of the maximum growth rate is quite accurately predicted. Unfortunately, our attempts at a numerical solution of (3.11), (3.12) with a reasonable number of grid points for the case $n = -15$, $M = 15$ proved unsuccessful, due to a large number of spurious (i.e. highly grid–dependent) modes. Indeed, it was found that as M was increased, our numerical scheme often failed abruptly, with a sudden generation of large numbers of spurious modes.

Referring again to figures 14, we see that the upper neutral point is clearly seen. This occurs at $\alpha = -n/q$, the point at which $a = 0$ (see (6.33)). The fully numerical results throughout this paper all very clearly show this result, which appears to apply universally, as in the incompressible case.

Additionally figures 14 show a distinct lower neutral point. This corresponds to the value of α where $\varphi_0''(0) = 0$ namely $\bar{\alpha} = -q/2$. At this location, a and b (defined by (6.33)) both exhibit a singularity. There is some correlation with these results and those of the fully numerical scheme. Indeed, it is most remarkable that the location of this lower neutral point is identical with that found in the incompressible case (Stewartson & Leibovich 1987), and that both the upper and lower neutral points are captured by (6.45).

It is also worth noting that there is some similarity between the structure of these modes, and those found in the incompressible work of Stewartson & Brown (1985), although the particular details are different, and in our case analytic/asymptotic solution on the $r = \mathrm{O}(1)$ scale is possible (see 6.6), whilst Stewartson & Brown (1985) had to resort to a numerical approach for this scale.

In the following subsection we go on to draw a number of conclusions from our study.

7. Conclusions

We have mounted a systematic study of the inviscid stability of the trailing line vortex, starting at zero Mach number M, and progressively increasing M. We see a general reduction in growth rates as M increases, and indeed the results of subsections 5.4 and 5.5 predict that the original family of modes will stabilise when $M = \mathrm{O}(|n|^{\frac{1}{2}})$, specifically when (5.43) is satisfied. However it is shown in section 6 that when $M = \mathrm{O}(|n|)$, a centre mode class of instability is formed. We feel that although our numerical results (figures 12 in particular) indicate that these modes spring from the higher order modes at lower Mach numbers, as $-n$ increases these centre modes modes may well become distinct from the original class of modes that exist at lower Mach numbers.

A further important feature of note, and one that is observed in incompressible work (Leibovich & Stewartson 1983, Stewartson & Brown 1985) is that there is a good deal of numerical evidence to suggest that there exist no instabilities for $\alpha > -n/q$. Indeed, this is also confirmed by (6.45), noting that a is given by (6.33). This aspect is currently under further investigation.

Acknowledgements

J.A.K.S was in receipt of a S.E.R.C. studentship. A number of the computations were performed with the computer facilities provided by the University of Manchester.

References

Batchelor, G.K. 1964 Axial flow in trailing line vortices. J. Fluid Mech. 20, 645

Coleman, C.S. 1989 The stability of swirling jets. Astro. Soc. Australia Proc. 8, 38

Duck, P.W. 1986 The inviscid stability of a swirling flow: large wavenumber disturbance. J. Appl. Math. Phys. (ZAMP) 37, 340

Duck, P.W. & Foster, M.R. 1980 The inviscid stability of a trailing line vortex. J. Appl. Math. Phys. (ZAMP) 31, 524

Duck, P.W. & Khorrami, M.R. 1991 On the effects of viscosity on the stability of a trailing line vortex. ICASE report 91-6 (To appear in J. Fluid Mech.)

Foster, M.R. & Duck, P.W. 1982 Inviscid stability of Long's vortex. Phys. Fluids 25, 1715

Foster, M.R. & Smith, F.T. 1989 Stability of Long's vortex at large flow force. J. Fluid Mech. 206, 405

Görtler, H. 1954 Theoretical investigations of laminar boundary–layer problems II— theory of swirl in an axially symmetric jet, far from the orifice. Air Force Contract no. AF 61(514) 627C

Khorrami, M.R. 1991 On the viscous modes of instability of a trailing line vortex. J. Fluid Mech. 225, 197

Khorrami, M.R., Malik, M.R. & Ash, R.I. 1989 Application of spectral collocation techniques to the stability of swirling flows. J. Comp. Phys. 81, 206

Leibovich, S. & Stewartson, K. 1983 A sufficient condition for the instability of columnar vortices. J. Fluid Mech. 126, 355

Lessen, M. & Paillet, F. 1974 The stability of a trailing line vortex. Part 2. Viscous theory. J. Fluid Mech. 65, 769

Lessen, M., Singh, P. & Paillet, F. 1974 The stability of a trailing line vortex. Part 1. Inviscid theory. J. Fluid Mech. 53, 753

Loitsyanskii, L.G. 1953 Propogation of a rotating jet in an infinite space surrounded by the same liquid. Prik. Mat. Mehk.17, 3

Michalke, A. 1971 Instabilitäteines Kompressiblen rundens Freistrahls inter Beruck-sichtingung des Einflusses den Strahlgrenzschtdicke. J. Flugwiss 19, 319

Michalke, A. 1984 Survey on jet instability theory. Prog. in Aeropace Sci. 21, 519

Stewartson, K. & Brown, S.N. 1984 Inviscid centre–modes and wall–modes in the stability theory of swirling Poiseuille flow. IMA J. Appl. Math. 32, 311

Stewartson, K. & Brown, S.N. 1985 Near neutral centre modes as inviscid perturbations to a trailing line vortex. J. Fluid Mech. 156, 387

Stewartson, K. & Capell, S. 1985 On the stability of ring modes in a trailing line vortex: the upper neutral points. J. Fluid Mech. 156, 369

Stewartson, K. & Leibovich, S. 1987 On the stability of a columnar vortex to disturbances with large azimuthal wavenumber: the lower neutral points. J. Fluid Mech. 178, 549

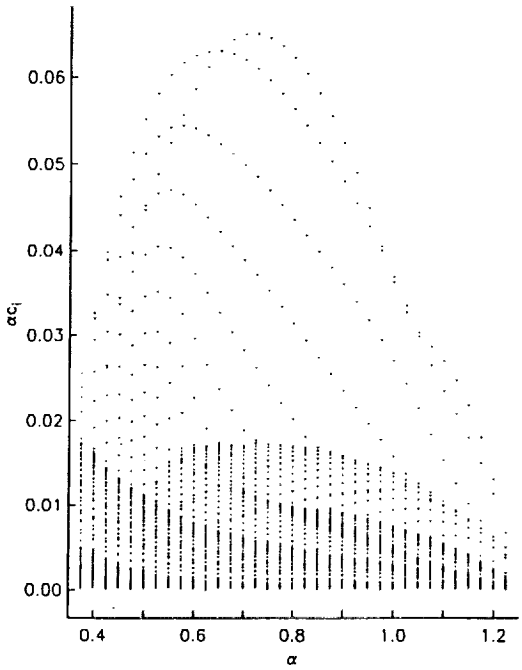

Figure 1a Variation of growth rate with α, $n = -1$, $M = 3$.

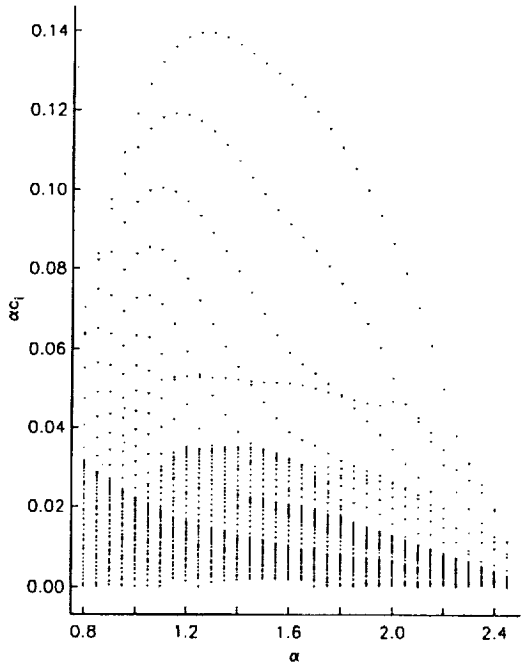

Figure 1b Variation of growth rate with α, $n = -2$, $M = 3$.

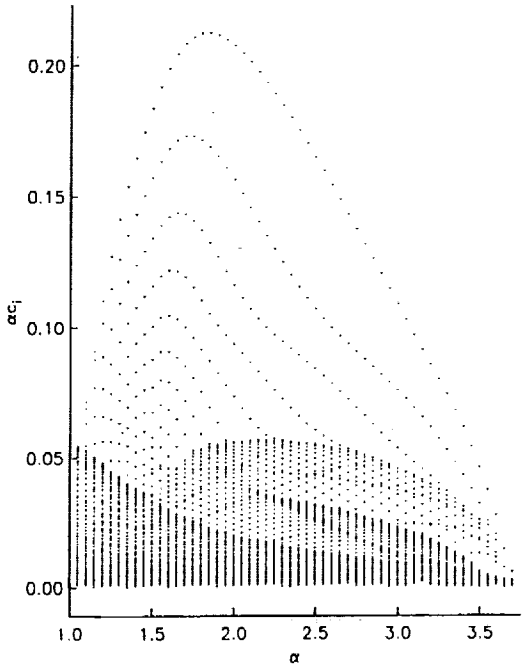

Figure 1c Variation of growth rate with α, $n = -3$, $M = 3$.

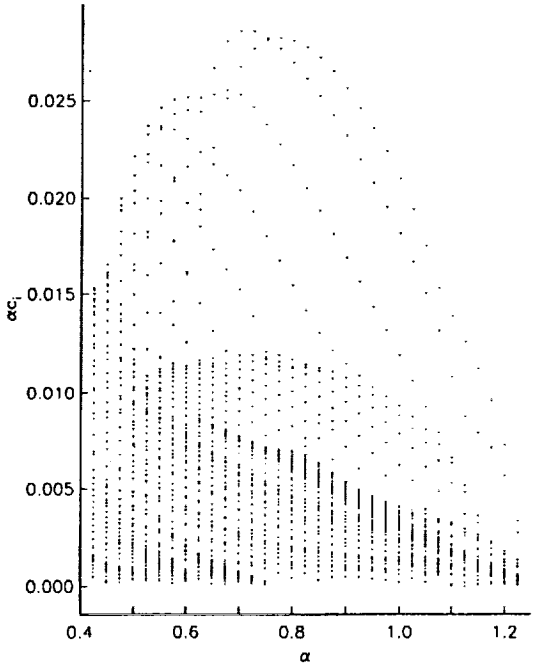

Figure 2a Variation of growth rate with α, $n = -1$, $M = 5$.

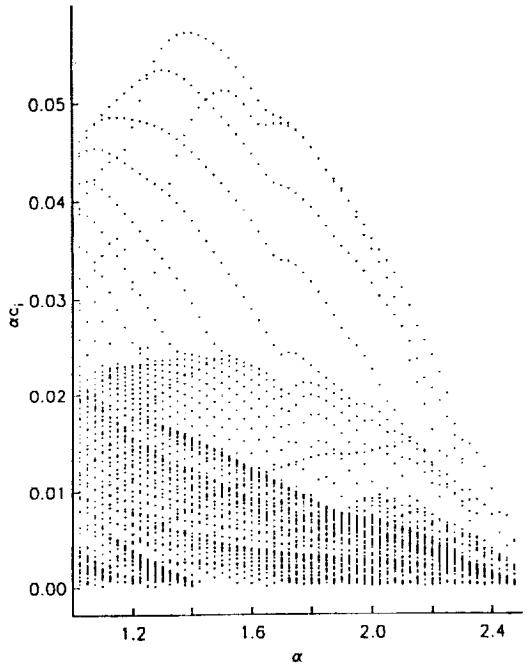

Figure 2b Variation of growth rate with α, $n = -2$, $M = 5$.

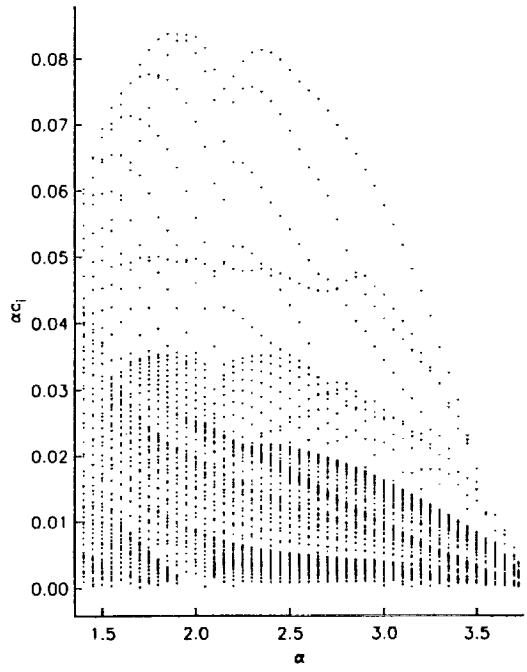

Figure 2c Variation of growth rate with α, $n = -3$, $M = 5$.

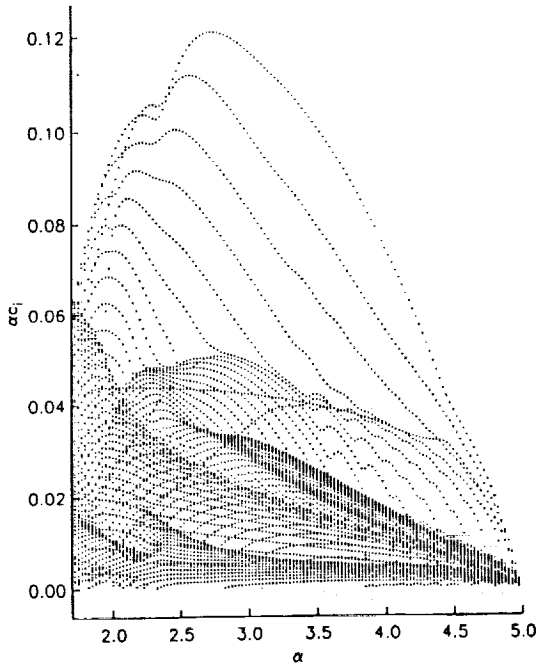

Figure 2d Variation of growth rate with α, $n = -4$, $M = 5$.

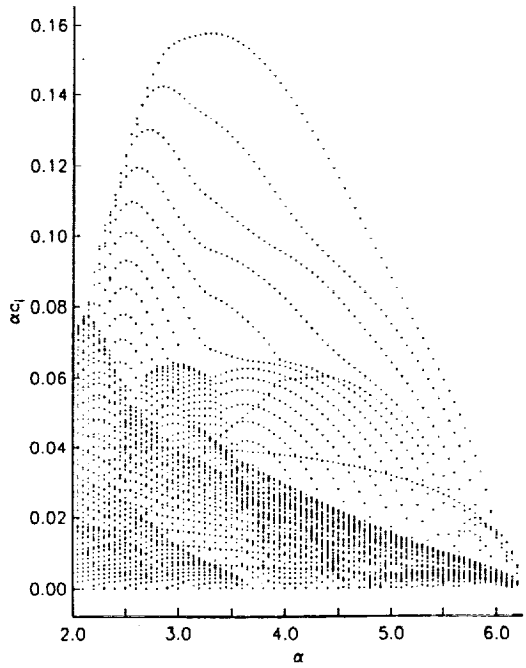

Figure 2e Variation of growth rate with α, $n = -5$, $M = 5$.

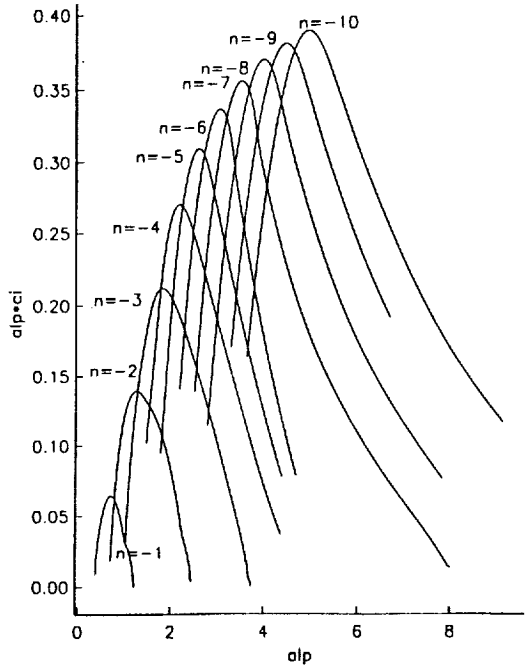

Figure 3 Variation of growth rate with α, computed most dangerous modes, $M = 3$, $n = -1$ through $n = -10$.

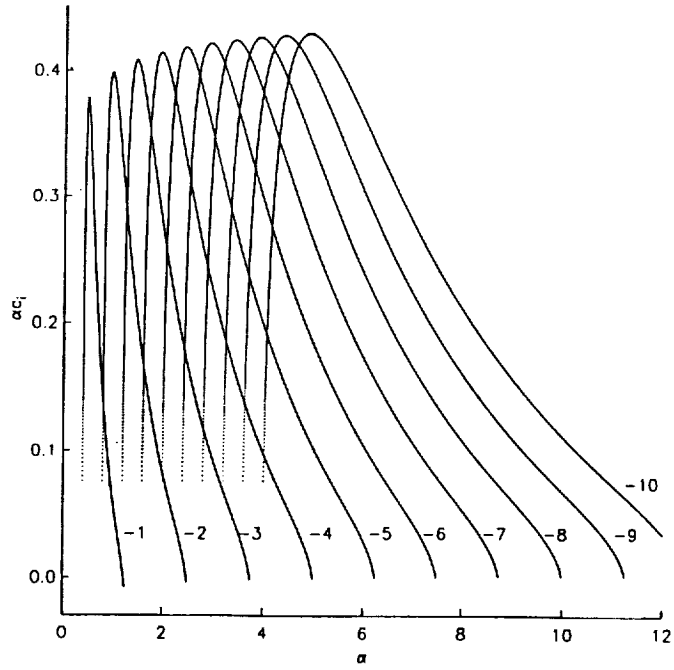

Figure 4 Variation of growth rate with α, asymptotic most dangerous modes using section 5.1 results, $M = 3$, $n = -1$ through $n = -10$.

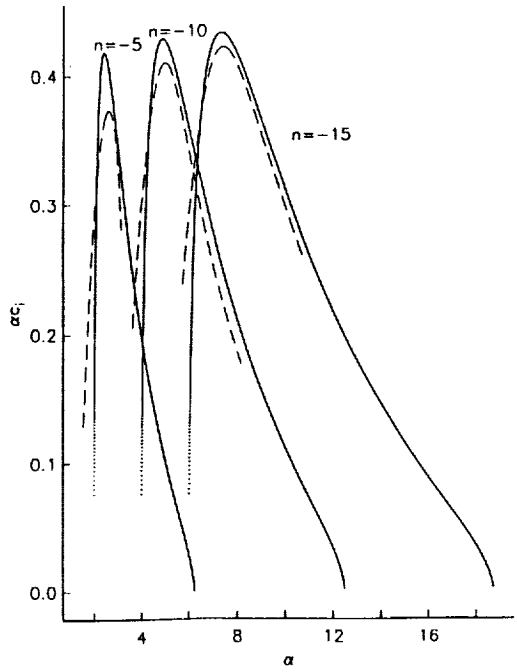

Figure 5 Variation of growth rate with α, for $n = -5, -10, -15$ $M = |n|^{\frac{1}{4}}$.

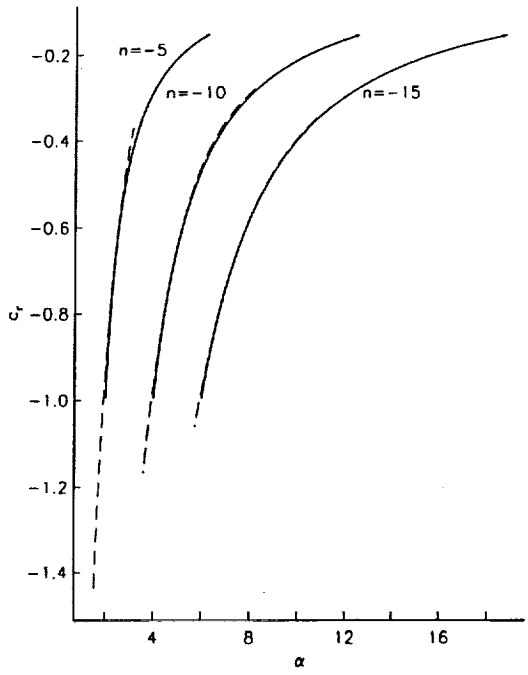

Figure 6 Variation of c_r with α, for $n = -5, -10, -15$ $M = |n|^{\frac{1}{4}}$.

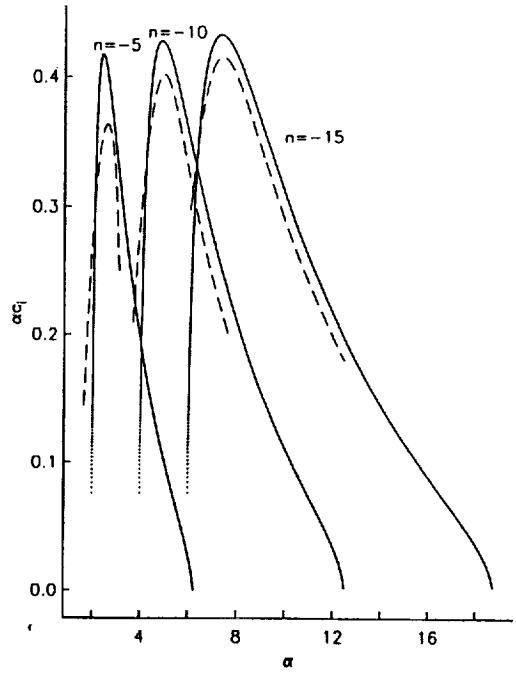

Figure 7 Variation of growth rate with α, for $n = -5, -10, -15$ $M = |n|^{\frac{3}{8}}$.

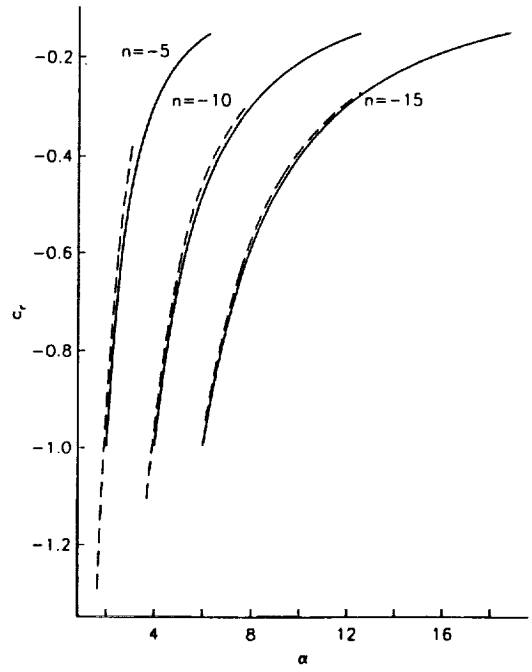

Figure 8 Variation of c_r with α, for $n = -5, -10, -15$ $M = |n|^{\frac{3}{8}}$.

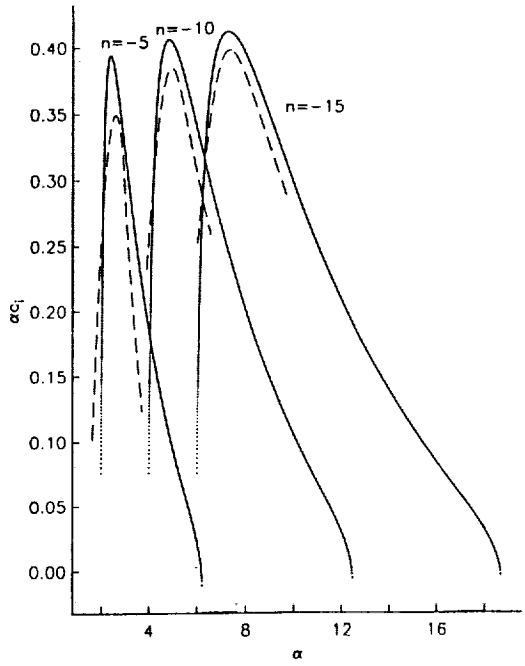

Figure 9 Variation of growth rate with α, for $n = -5, -10, -15$ $M = |n|^{\frac{1}{2}}$.

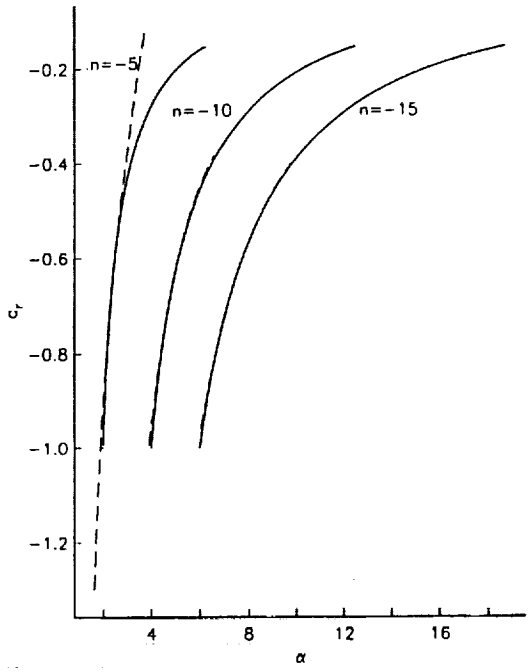

Figure 10 Variation of c_r with α, for $n = -5, -10, -15$ $M = |n|^{\frac{1}{2}}$.

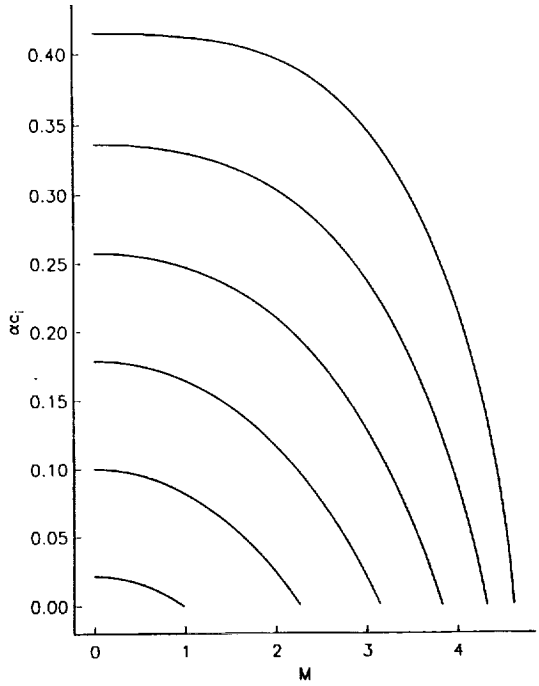

Figure 11a Variation of growth rate with M using section 5.4 results, $n = -5$, $\alpha = 2.5$, first 6 modes.

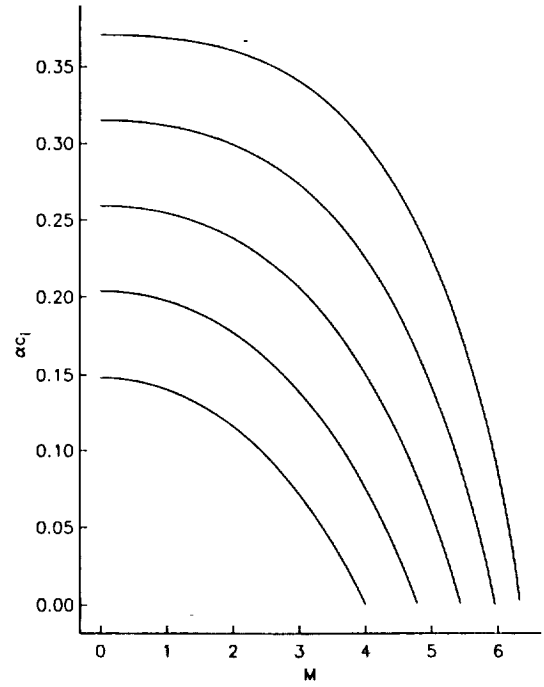

Figure 11b Variation of growth rate with M using section 5.4 results, $n = -10$, $\alpha = 5$, first 6 modes.

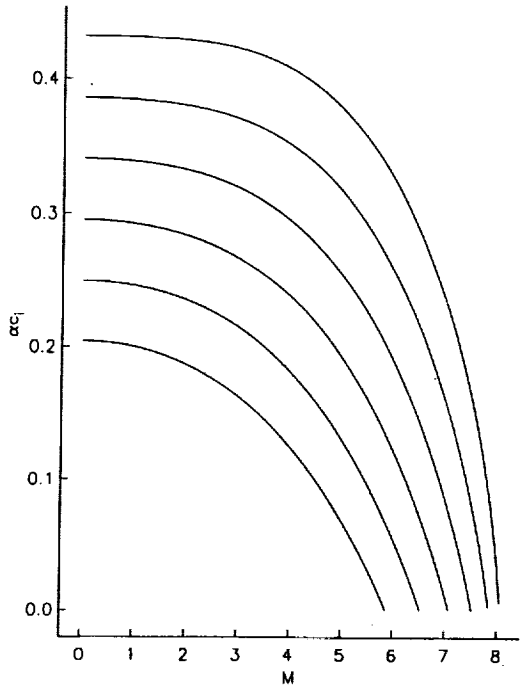

Figure 11c Variation of growth rate with M using section 5.4 results, $n = -15$, $\alpha = 7.5$, first 6 modes.

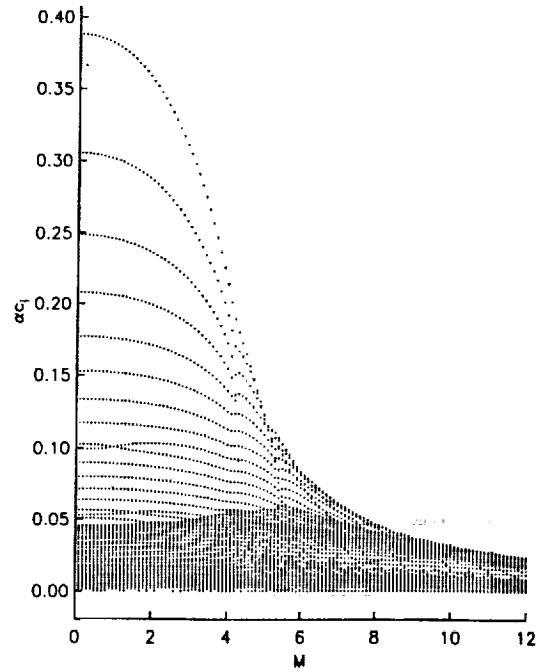

Figure 12a Variation of growth rate with M fully numerical results, $n = -5$, $\alpha = 2.5$, first 6 modes.

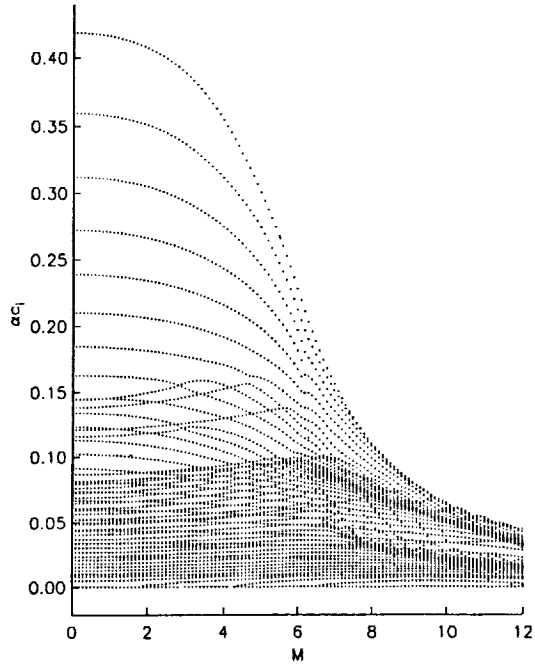

Figure 12b Variation of growth rate with M fully numerical results, $n = -10$, $\alpha = 5$, first 6 modes.

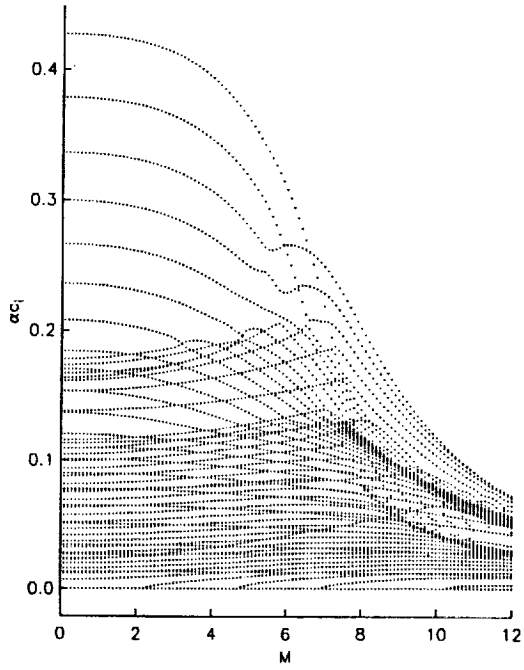

Figure 12c Variation of growth rate with M fully numerical results, $n = -15$, $\alpha = 7.5$, first 6 modes.

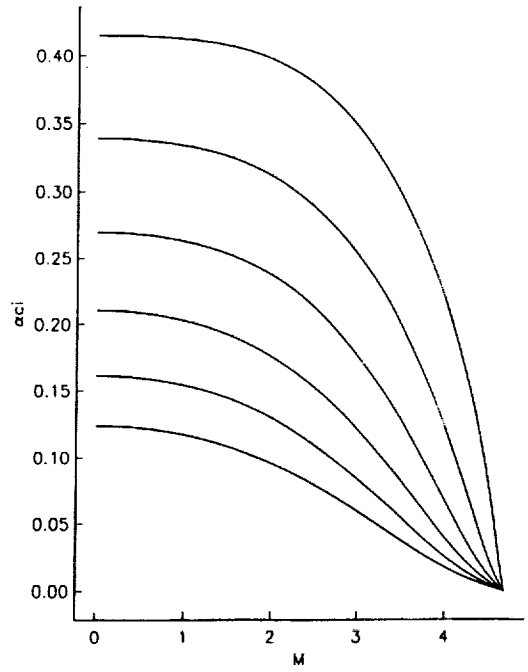

Figure 13a Variation of growth rate with M using section 5.5 results, $n = -5$, $\alpha = 2.5$, first 6 modes.

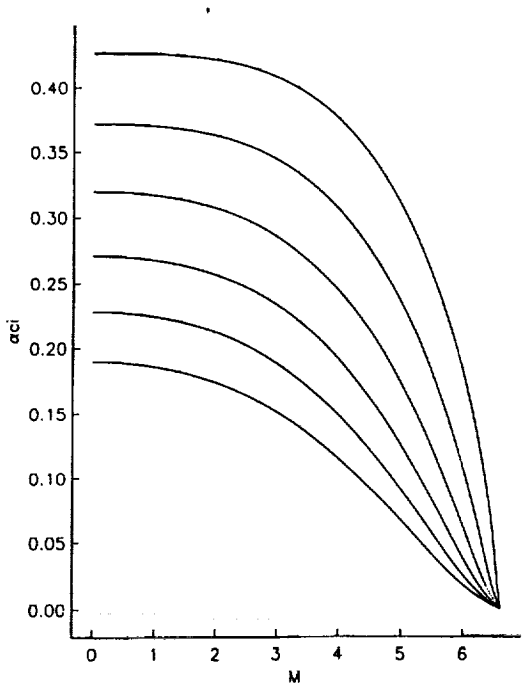

Figure 13b Variation of growth rate with M using section 5.5 results, $n = -10$, $\alpha = 5$, first 6 modes.

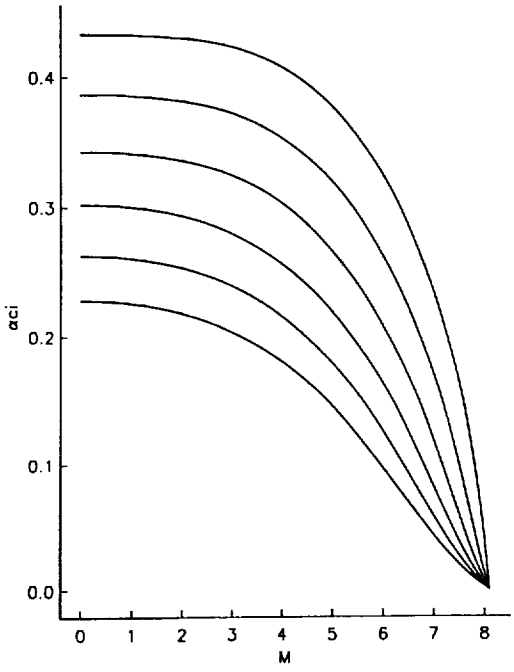

Figure 13c Variation of growth rate with M using section 5.5 results, $n = -15$, $\alpha = 7.5$, first 6 modes.

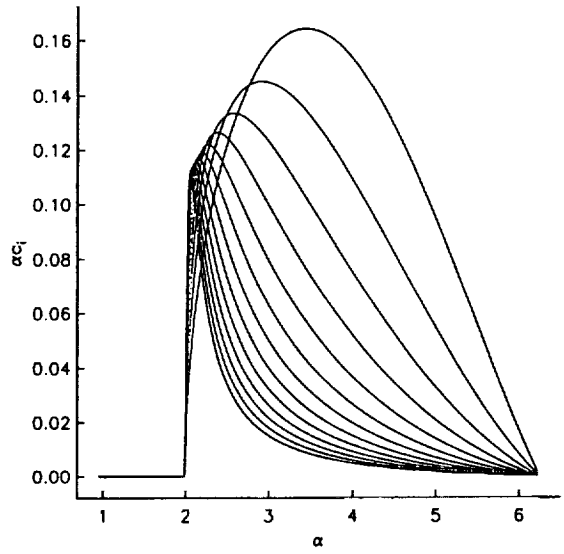

Figure 14a Variation of growth rate with α for centre modes, $n = -5$, $M = 5$.

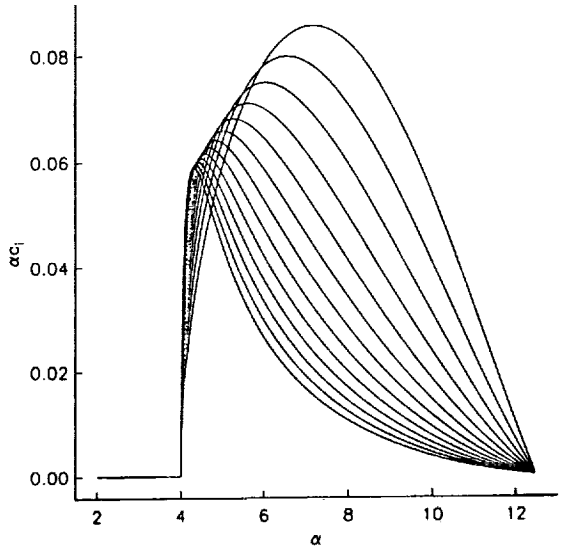

Figure 14b Variation of growth rate with α for centre modes, $n = -10$, $M = 10$.

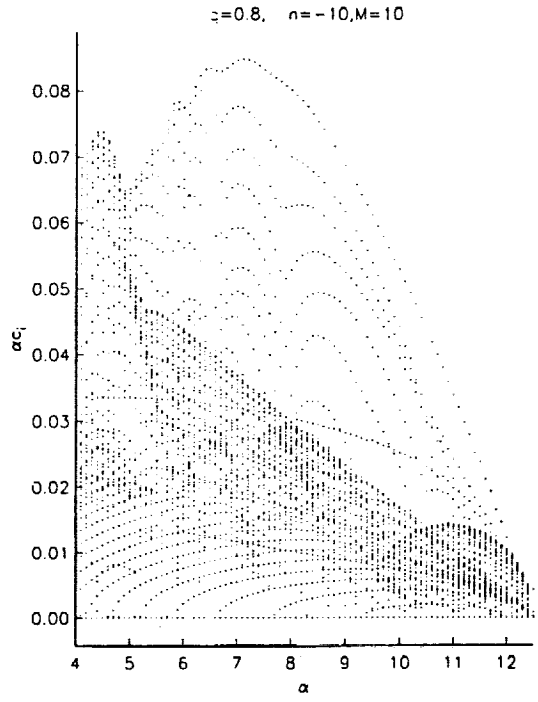

Figure 15 Variation of growth rate with α $n = -10$, $M = 10$, fully numerical results.

REPORT DOCUMENTATION PAGE

Form Approved
OMB No 0704-0188

1. AGENCY USE ONLY (Leave blank)	2. REPORT DATE	3. REPORT TYPE AND DATES COVERED
	December 1992	Contractor Report

4. TITLE AND SUBTITLE

THE STABILITY OF A TRAILING-LINE VORTEX IN COMPRESSIBLE FLOW

5. FUNDING NUMBERS

C NAS1-18605
C NAS1-19480

WU 505-90-52-01

6. AUTHOR(S)

Jillian A. K. Stott
Peter W. Duck

7. PERFORMING ORGANIZATION NAME(S) AND ADDRESS(ES)

Institute for Computer Applications in Science and Engineering
Mail Stop 132C, NASA Langley Research Center
Hampton, VA 23681-0001

8. PERFORMING ORGANIZATION REPORT NUMBER

ICASE Report No. 92-65

9. SPONSORING / MONITORING AGENCY NAME(S) AND ADDRESS(ES)

National Aeronautics and Space Administration
Langley Research Center
Hampton, VA 23681-0001

10. SPONSORING / MONITORING AGENCY REPORT NUMBER

NASA CR-189738
ICASE Report No. 92-65

11. SUPPLEMENTARY NOTES

Langley Technical Monitor: Michael F. Card
Final Report

Submitted to Journal of Fluid Mechanics

12a. DISTRIBUTION / AVAILABILITY STATEMENT

Unclassified - Unlimited

Subject Category 02

12b. DISTRIBUTION CODE

13. ABSTRACT *(Maximum 200 words)*

We consider the inviscid stability of the Batchelor (1964) vortex in a compressible flow. The problem is tackled numerically and also asymptotically, in the limit of large (aximuthal and streamwise) wavenumbers, together with large Mach numbers. The nature of the solution passes through different regimes as the Mach number increases, relative to the wavenumbers. At very high wavenumbers and Mach numbers, the mode which is present in the incompressible case ceases to be unstable, whilst new "centre mode" forms, whose stability characteristics are determined primarily by conditions close to the vortex axis. We find that generally the flow becomes less unstable as the Mach number increases, and that the regime of instability appears generally confined to disturbances in a direction counter to the direction of the rotation of the swirl of the vortex.

Throughout the paper comparison is made between our numerical results and results obtained from the various asymptotic theories.

14. SUBJECT TERMS

inviscid, vortex, stability

15. NUMBER OF PAGES

54

16. PRICE CODE

A04

17. SECURITY CLASSIFICATION OF REPORT	18. SECURITY CLASSIFICATION OF THIS PAGE	19. SECURITY CLASSIFICATION OF ABSTRACT	20. LIMITATION OF ABSTRACT
Unclassified	Unclassified		